

# **DLR-IB-FA-BS-2020-75**

**Determination of local loads for  
the testing of subcomponents of a  
wind turbine blade**

**Masterarbeit**

Abdullah Ejaz Mir  
Christian Willberg



DLR

Deutsches Zentrum  
für Luft- und Raumfahrt



Institut für Faserverbundleichtbau und Adaptronik

**DLR-IB-FA-BS-2020-75**

**Determination of local loads for the testing of  
subcomponents of a wind turbine blade**

**Zugänglichkeit:**

**Stufe 1 Allgemein zugänglich:** Der Interne Bericht wird elektronisch ohne Einschränkungen in ELIB abgelegt. Falls vorhanden, ist je ein gedrucktes Exemplar an die zuständige Standortbibliothek und an das zentrale Archiv abzugeben.

Braunschweig, Juni, 2020

Abteilungsleiter:  
Dr.-Ing. Tobias Wille



Der Bericht umfasst: 117 Seiten

Autoren:  
M. Sc. Abdullah Ejaz Mir



Dr.-Ing. Christian Willberg



DLR

  
Deutsches Zentrum  
für Luft- und Raumfahrt

# **Determination of local loads for the testing of subcomponents of a wind turbine blade.**

## **Master Thesis**

Degree Program: Computational Engineering  
Faculty of Civil and Environmental Engineering, Ruhr-University Bochum

**Abdullah Ejaz Mir**

from Lahore, Pakistan  
Registration Number: 1080 1625 6047

**6th-May 2020**

**1<sup>st</sup> Examiner: Prof. Dr. rer. nat. Klaus Hackl**

Department of mechanics-material theory  
Ruhr University Bochum

**2<sup>nd</sup> Examiner: Dr.-Ing. Ulrich Hoppe**

Department of mechanics-material theory  
Ruhr University Bochum

**Supervisor: Dr.-Ing. Christian Willberg**

Institute for fiber composite lightweight structures and  
adaptronics  
German Aerospace Center, Braunschweig

## **Declaration of authorship**

I declare that I have completed this work as my master thesis under supervision of Dr.-Ing. Christian Willberg.

The information that has been directly or indirectly taken from other sources has been referenced accordingly. The current work has not been published or presented to an examination committee before.

---

Date, Signature

## **Acknowledgements**

I am thankful to Allah almighty, who has endowed me this blessing. I would like to express my gratitude to my supervisor Dr.-Ing. Christian Willberg, for providing me an opportunity to write my master thesis at German Aerospace Centre (DLR), Braunschweig. His suggestion guidance and fair check on my work honed my knowledge in the field and were paramount to achieving the objectives of the thesis. His close attention & proper guidance enabled me to work in the right direction throughout the thesis.

I would like to thank Prof. Dr. rer. nat. Klaus Hackl and Dr.-Ing. Ulrich Hoppe for their interest in this topic and for being the examiners.

Finally, I am obliged to all my colleagues for their support and cooperation throughout my work at DLR.

## **Abstract**

Verification of structures through testing and simulation of subsections is a technique used in structural mechanics. Wind turbine rotor blades are large constructs and their testing demands spatial testing facilities and expensive tooling. The project aims to develop a verification protocol for wind turbine rotor blade using numerical simulation of a subsection, from within the blade. All research conducted is concerning the latest trend in wind turbine design that incorporates smart blades. A transfer scheme is developed, that transfers the loads of the blade (as generated during testing of the complete blade) to a subsection loads (which can be applied via test bench), and vice versa. The required degree of freedoms for a test bench to completely replicate the stress state within the subsection has been determined. The possibility of replication of stress state on a machine, currently present at the “German aerospace centre”, has been ruled out. Furthermore, a methodology to permit replication of the stress state along one axis has been documented. The protocol developed is intended to eliminate spatial and tooling requirement for testing of rotor blades.

# Table of Contents

Declaration of authorship .....	1
Acknowledgements .....	2
Abstract .....	3
Table of Contents .....	4
List of Tables .....	9
Chapter-1: Introduction.....	10
1.1 State of the art .....	10
1.2 Objective .....	12
Chapter 2-Literature review .....	15
2.1 Numerical modelling .....	15
2.1.1 Material & Mechanics.....	15
2.1.2 FEM theoretical insight.....	19
2.1.3 Solid / Volume element .....	20
2.1.4 Shell element.....	21
2.1.5 Mass 21 element and constraint equation formulation .....	23
2.1.6 Coupling degree of freedoms.....	25
2.1.7 Modelling with multiple meshes.....	26
2.2 Testing of wind turbines .....	27
Chapter 3-Experimental and numerical setup.....	30
3.1Experimental setup .....	30
3.1.1 Details & Specification .....	30
3.1.2 Loading capability.....	32
3.2 Numerical setup .....	33
3.2.1 Model description .....	36
3.2.2 Transfer matrix extraction.....	40
3.2.3 Implementation of boundary condition.....	42
Chapter 4-Results .....	43
4.1Transfer Matrix .....	43

4.1.1 Reaction loads/Resulting deformation to transfer matrix .....	43
4.1.2 Matrix Robustness test .....	45
4.2 Boundary condition verification .....	47
4.2.1 Threaded pallets modelling .....	47
4.3.1 Direct generation method .....	49
4.3.1 (A) Replicate complete stress state .....	49
4.3.1(B) possible load case- dual sided load introduction .....	50
4.3.1 (C) preferable load case- Single sided load introduction. ....	52
4.3.1(D) Single sided load introduction with axial displacement.....	53
4.3.2 Function fitting and optimization .....	58
Chapter-5: Conclusion & future work .....	60
Appendix .....	62
Bibliography.....	83



## List of figures

Figure 1- Up scaling of wind turbine rotor diameter.[3] .....	10
Figure 2: All possible load cases on the test rig(a)Bending pressure load, (b)Bending tension load, (c)Bending dominant, (d)Shear dominant load.....	13
Figure 3: Cross section of a wind turbine blade.[7].....	15
Figure 4: Spar nomenclature.[11] .....	16
Figure 5: Typical spar layouts.[10] .....	16
Figure 6: Sections bonded by adhesives in wind turbine blades.[12] .....	17
Figure 7: wind turbine blade with the different airfoil sections.[13].....	18
Figure 8: Sample layup plan for a blade (Section-1 on display).[14].....	18
Figure 9:Dirichlet and Neumann boundary conditions.[16] .....	20
Figure 10: SOLID186element.[17].....	21
Figure 11: Geometry of Shell 281 element.[19] .....	22
Figure 12: Geometry of a Mass21 element.[20] .....	23
Figure 13:Relationship between rotational and translational DOF's.[20].....	25
Figure 14: CAD-Model of test bench currently present at DLR. ....	30
Figure 15: Test bench currently present at DLR. ....	31
Figure 16: Extension of possible load set via translation of specimen.....	32
Figure 17: Extension of possible load set via rotation of specimen. ....	32
Figure 18: Reference plane and stacking direction.....	37
Figure 19: Solid and shell distribution.....	38
Figure 20: Coordinate system of blade. ....	40
Figure 21: Transfer matrix & machine load extraction (refer to fig. 16 & 17). .	41
Figure 22: Rigid constraints between master and slave nodes. ....	41
Figure 23: Transfer matrices for a displacement controlled test. ....	44
Figure 24: Robustness test output (Test type: Force controlled, variation along Y-axis: 100 mm, variation along Z-axis: 100 mm). ....	46
Figure 25: Robustness test output(Test type: Displacement controlled, variation along Y-axis: 100 mm, variation along Z-axis: 100 mm). ....	47
Figure 26: Element table output for threaded pallet deformation. ....	48

Figure 27: Illustration of how axial deformation could be incorporated.....	54
Figure 28: Coupling identification(1). .....	56
Figure 29: Coupling identification(2). .....	57
Figure 30: Transfer matrix for force controlled test (X-coordinate: 2000) .....	63
Figure 31: Transfer matrix for force controlled test (X-coordinate: 4000) .....	64
Figure 32: Transfer matrix for force controlled test (X: 8000) .....	65
Figure 33: Transfer matrix for force controlled test (X: 16000) .....	66
Figure 34: Transfer matrix for displacement controlled test (X: 2000) .....	67
Figure 35: Transfer matrix for displacement controlled test (Xcoordinate4000) .....	68
Figure 36: Transfer matrix for displacement controlled test (Xcoordinate8000) .....	69
Figure 37: Transfer matrix for displacement controlled test (Xcoordinate16000) .....	70
Figure 38: Robustness test output (type: displacement controlled, test load case from: first column of transfer matrix, amplification factor: 1) .....	71
Figure 39: Robustness test output (type: displacement controlled, test load case from: second column of transfer matrix, amplification factor: 1) .....	72
Figure 40: Robustness test output (type: displacement controlled, test load case from: third column of transfer matrix, amplification factor: 1) .....	73
Figure 41: Robustness test output (type: displacement controlled, test load case from: fourth column of transfer matrix, amplification factor: 1) .....	74
Figure 42: Robustness test output (type: displacement controlled, test load case from: fifth column of transfer matrix, amplification factor: 1) .....	75
Figure 43: Robustness test output (type: displacement controlled, test load case from: sixth column of transfer matrix, amplification factor: 1) .....	76
Figure 44: Robustness test output (type: force controlled, test load case from: first column of transfer matrix, amplification factor: 1) .....	77
Figure 45: Robustness test output (type: force controlled, test load case from: second column of transfer matrix, amplification factor: 1) .....	78
Figure 46: Robustness test output (type: force controlled, test load case from: third column of transfer matrix, amplification factor: 1) .....	79

Figure 47: Robustness test output (type: force controlled, test load case from: fourth column of transfer matrix, amplification factor: 1) .....	80
Figure 48: Robustness test output (type: force controlled, test load case from: fifth column of transfer matrix, amplification factor: 1) .....	81
Figure 49: Robustness test output (type: force controlled, test load case from: sixth column of transfer matrix, amplification factor: 1) .....	82

## List of Tables

Table 1: Change in blade failure mode due to scaling(R is blade length).[5] ....	11
Table 2: Materials for various sections of wind turbine blades.[9] .....	16
Table 3: Load cases for static testing.[4] .....	29
Table 4: Technical specifications of hydraulic cylinders. ....	31
Table 5: Inputs for the model.....	33
Table 6: Model classes and respective outputs.....	36
Table 7: Materials used in modelling the 20meter specimen. ....	39
Table 8: Material numbers/labels in ANSYS APDL.....	39
Table 9: Stress state comparison between complete blade and specimen (1). ...	50
Table 10: Stress state comparison between complete blade and specimen(2). ..	51
Table 11: Stress state comparison between complete blade and specimen(3). ..	52
Table 12:Stress state comparison between specimen, with and without axial deformation within the system.....	55
Table 13: Difference in applied and resulting rotations (two rotations applied simultaneously). ....	56
Table 14: Measured rotations.....	58
Table 15: Material properties of 20-meter specimen.....	62

# Chapter-1: Introduction

## 1.1 State of the art

A wind turbine is a rotary engine that converts kinetic energy of a moving fluid to mechanical energy. It accomplishes this task by rotating a bladed rotor using moving fluid flowing across the skin of rotor blade.[1] A wind turbine comprises of many dedicated components, each playing a vital role in the power conversion process. The rotor blades are one of the vital components of the wind turbine and engineering challenges posed in their development, range from blade design, material selection, manufacturing, metrology and testing.

Wind turbines come with power ratings. The size of the rotor blade is directly related to the power output of the turbine. The focus of turbine manufacturing sector is on increasing size of the rotor blade to ramp up power output per turbine and cut down on farm size. [3]

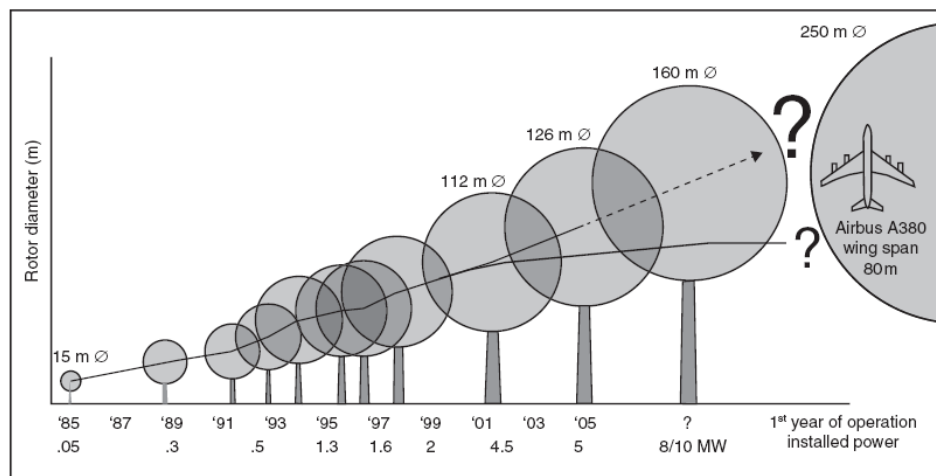


**Figure 1- Up scaling of wind turbine rotor diameter.**[3]

Due to the enormous size of wind turbine blades the testing phase is an engineering feat. First, the load cases are deciphered by taking into consideration every possible load the blade can experience in its lifetime, for example lifting of the blade via crane during installation phase is a separate load case. A single load spectrum comprising of all possible load cases is created

and the critical load peaks are identified, and act as testing loads. These test loads are carried forward to the testing hall for verification of the rotor blade. Size of the testing facility is decided as per the size of the blade. The root of the blade is fixed to a custom designed mount, clamped to the ground. The loads are controlled via hydraulics fitted to a fixture, mounted to the ground as well. The hydraulics operates loading cables that transfer force to load frames which are clamped to the blade. The data for load, displacement and stress is recorded via load cells, draw wire sensors and strain gauges, respectively.[4] With passage of time, the span of wind turbine blades and their testing cost increases. The testing of a new generation of rotor blades leads to development of new testing equipment. Installation and calibration of the equipment is costly in both finances and time. The need for developing new testing halls is a constant issue because prior facilities may not be capable of housing future blades. With every new generation of blades all or some previous testing equipment also retires because it is incapable of coping up with the size of new blades.

***Table 1: Change in blade failure mode due to scaling(R is blade length). [5]***

Effects due to blade scaling				Blade Length			
	Design Driver	Critical Area	Scaling Law	30m	60m	90m	120m
Load	Aerodynamic loads	Cap	$F_{aero} \sim R^2$	5	4	3	2
	Gravity loads	Root, TE	$F_{grav} \sim R^3$	3	4	5	5
	Centrifugal load	No critical	$F_{cent} \sim R$	2	1	0	0
Load case	Bending flapwise	Brazier	Caps	3	4	5	5
		Buckling	Cap	5	4	3	3
		Tip Deflection	Tip	5	4	3	2
	Bending edgewise	Stiffness (resonance)	Root, transition	3	4	5	5
	Torsion	Flutter		2	3	4	4
	Bending flapwise+edgewise	Buckling+Distortion	Cap+Cross sec.	3	4	5	5
(failure) mode	Bending flapwise+edgewise+torsion	Distortion+Flutter	Cap+Cross sec.	3	4	5	5
	Interlaminar failure caused by Brazier	Caps		3	4	5	5
	Buckling	Cap		5	4	3	3
	Tip deflection	Tip		5	4	3	2
	Transverse Shear Distortion	Cross section		1	2	3	4
	Web failure	Webs		2	3	3	4
	Fatigue failure in root connection	Root	$F_{root} \sim R^4$	3	4	5	5
	Fatigue failure in root transition area	Transition area	$F_{root} \sim R^4$	3	4	5	5
	Fatigue failure in the bondlines	Bondl.in TE area	$F_{grav} \sim R^3$	3	4	5	5
	Flutter	Entire blade		1	2	3	4
	Trailing edge Buckling	Trailing edge	$F_{grav} \sim R^3$	3	4	5	5

Alongside the expenses is the risk aspect. The blade undergoes testing in a manner which only allows a certain number of load cases to be physically carried out. The fact of the matter is that along the span and chord of the rotor blade, various sections have different critical load cases (for example referring to “Table 1”, we see that for a blade length of 30-meters and flap wise bending, the tip and the cap are the critical areas/sections). To physically apply critical loads to certain sections is not possible given the current testing methodology, of testing the complete blade at once. Thus, data concerning response of the blade to section specific critical loads is missing even after testing the complete blade. Similarly, to test a number of sections until failure is not possible with this methodology of testing. So there is missing information even after testing because data concerning failure loads of various sections is not extracted through complete blade testing. Developing a verification methodology for rotor blades which is independent of size of the rotor blade is the task of this project.

## *1.2 Objective*

The aim of the thesis is to come up with a transfer scheme that can transfer the global loads, from a complete blade test, to local loads (equivalent loads), to be applied on a testing rig/test bench, for verification of subsections of rotor blade.

Various steps involved are:

- Development of a transfer scheme for relating internal loads of a subsection to loads acting upon the actual blade and vice versa.
- Modelling the testing protocol of the subsection (subcomponent) in ANSYS APDL, for a testing rig formerly present at “German Aerospace Centre” (DLR).
- A methodology is discussed and implemented to retrace back to the loading state of the actual blade, from the stress state of the subsection.

- Automation of the modelling work. The model will require parametric data such as locations where to section the blade, the location of sensors etc. (The script has to be structured in a way that all data checks are displayed only on request)

The test bench (currently present at DLR) has its limitations. It can only apply a certain set of loads. All possible combinations of loading incorporate a bending load. There is no possibility to generate a pure torsion, tension or compression load, as clear from figure below.

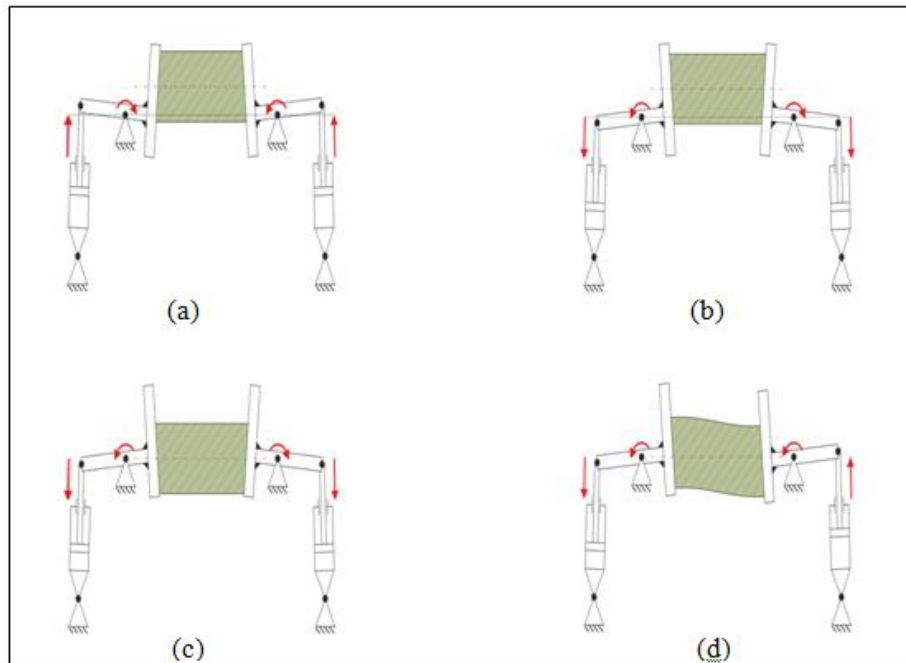


**Figure 2: All possible load cases on the test rig(a)Bending pressure load, (b)Bending tension load, (c)Bending dominant, (d)Shear dominant load**

The project involves developing a correlation between practical and numerical work, and it is important to include state of the art of both. A literature review has been conducted, covering both aspects involved in the project. In the beginning, the details of the numeric's involved in the setup of the model are discussed including the concepts of solid mechanics, finite element methods, modelling elements and transformation scheme. Then, some testing protocols for structural verification of wind turbine blades currently in practice are discussed. The test rig and the numerical setup of the simulation are discussed



in further details, ahead in the report, leading to the results section. In the final section future prospects of the project are discussed.

Note that all research conducted is as per the latest trend in blade design, so called “smart blades”. Smart blades, are class of wind turbine blades that tend to alter their profile as per wind conditions.

## Chapter 2-Literature review

### 2.1 Numerical modelling

#### 2.1.1 Material & Mechanics

A wind turbine blade is a shell type construct, hollow from inside. The rotor blade comprises of an outer skin supported by one or more spars (structural beams). The entire assembly is held together via adhesive joints. The number of spars used for reinforcement and their shape (I-beam or box type), depends upon the size of the blade. [6]

A typical cross section of a wind turbine blade is shown in figure below:[7]

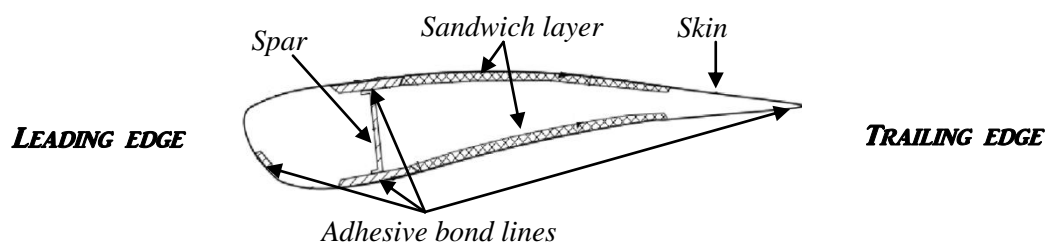


**Figure 3: Cross section of a wind turbine blade.** [7]

Due to the spacious design of rotor blades the mass of the blade is an issue itself. The environment in which the wind turbines operate is not lenient in its oxygen and moisture content, so the corrosion factor comes into the equation as well. The maintenance issues of such a colossal component also play a decisive role in material selection phase. All these factors put forth constitute the material selection considerations for rotor blades i.e. the material to be used for rotor blade manufacturing shouldn't just be strong it should be cheap, lightweight, corrosion resistant and easily repairable. [14] [8]

Below mentioned is a table of material options available for construction of wind turbine blades:[9]

**Table 2: Materials for various sections of wind turbine blades. [9]**

Section	Material options		
<i>Spar &amp; Skin</i>	<i>Fiber reinforced plastics (FRP)</i>	<b>Fibers options</b>	<b>Matrix options</b>
		<i>Glass</i>	<i>Thermoset</i>
		<i>Carbon</i>	<i>Thermoplastics</i>
		<i>Aramid</i>	<i>Nanoengineered polymers &amp; composites</i>
		<i>Basalt</i>	-
		<i>Hybrid</i>	-
		<i>Natural</i>	-
<i>Adhesive</i>	<i>Epoxy adhesives</i>	-	-
	<i>Polyurethane adhesives</i>	-	-
	<i>Methyl methacrylate adhesives</i>	-	-
	<i>Vinylester adhesives</i>	-	-

The spar section takes the lift load similar to one found in aircrafts. The spar is made out of composite material. The spar web is made out of multi axial layup of composites and the spar flange, typically referred to as spar cap, is made out of unidirectional composites.[10] Nomenclature and typical layouts of spars are shown in figures below: [11]

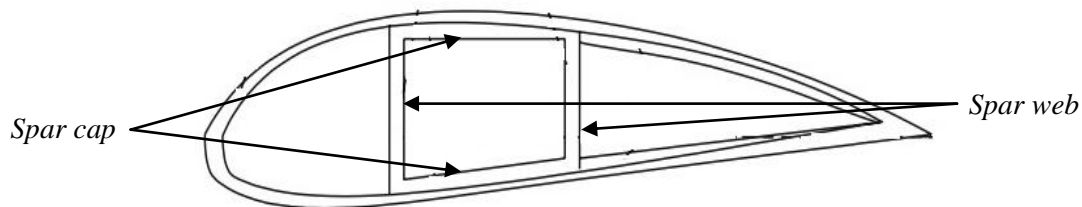


**Figure 4: Spar nomenclature. [11]**

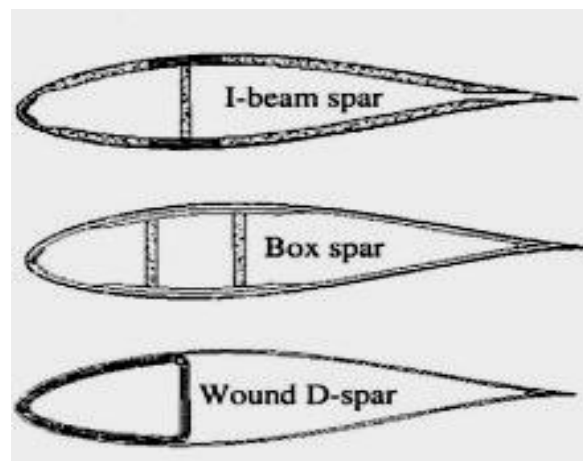


**Figure 5: Typical spar layouts. [10]**

Adhesives used in wind turbines are structural adhesives. They comprise of two constituent; a thermosetting resin and a hardener. Sometimes fillers are added or heat treatment is carried out to alter certain properties such as toughness, shrinkage etc. Below added is a picture highlighting areas bonded using adhesives.[12]

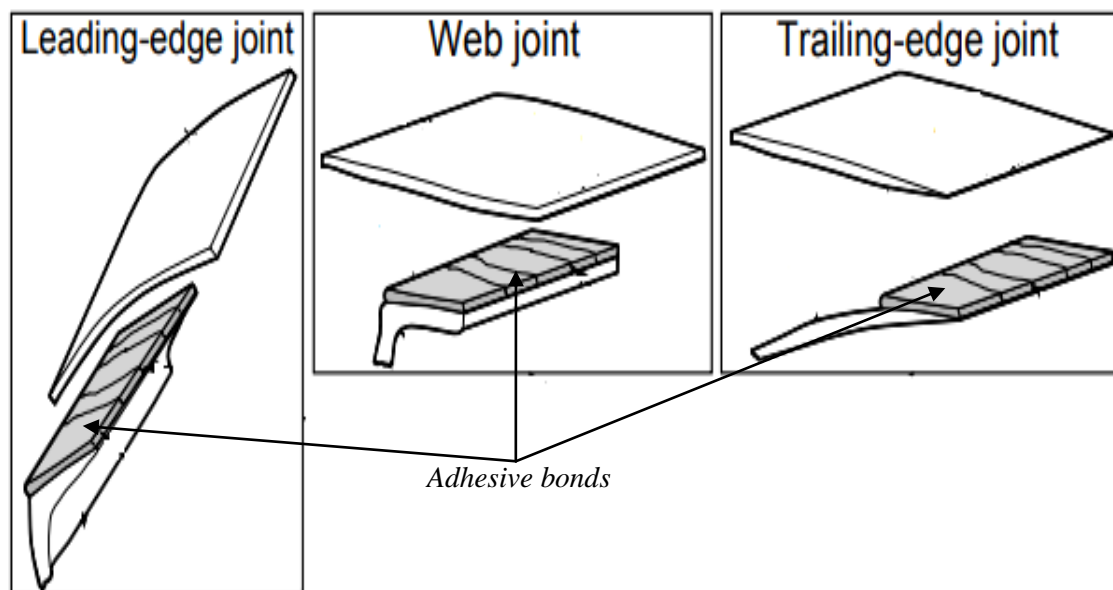


**Figure 6: Sections bonded by adhesives in wind turbine blades.** [12]

From 1970's it has been a standard to construct wind turbine blades from composite material for example carbon-epoxy laminate, glass-vinylester laminate, and polyvinyl chloride (PVC) foam. As individual sections of the blade have different loading histories (cyclic), the idea to have different materials at different areas/sections, for improving structural efficiency of the blade, is a viable one. Similarly, various sections of the blade possess a different profile as different profiles are better at performing different tasks, for example one could be better for structural purposes and another for aerodynamic efficiency. Some profiles are added between two profiles for smoothening the profile transition. [13]

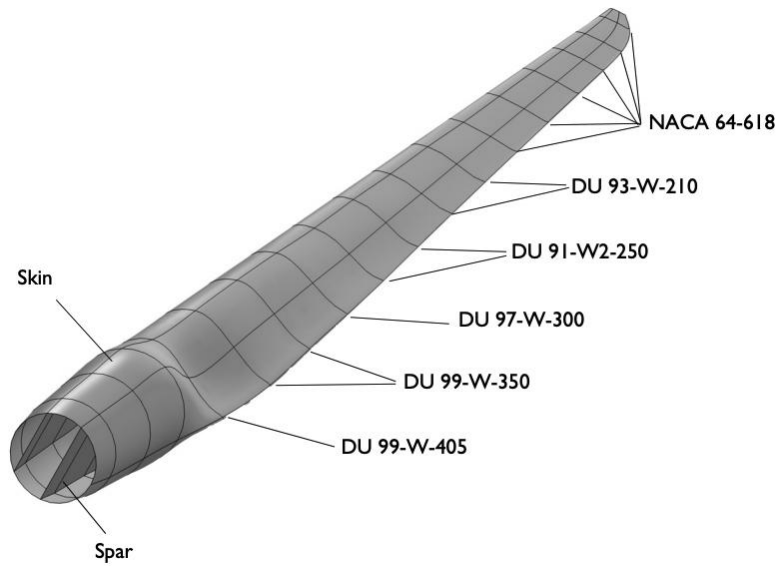


**Figure 7: wind turbine blade with the different airfoil sections.** [13]

Alongside, material alteration one can also vary the orientation and thickness of a composite layup, at various sections, to achieve desired strength requirements. A pictorial example of varying layups and thickness across the span of a wind turbine blade is provided below:[14]

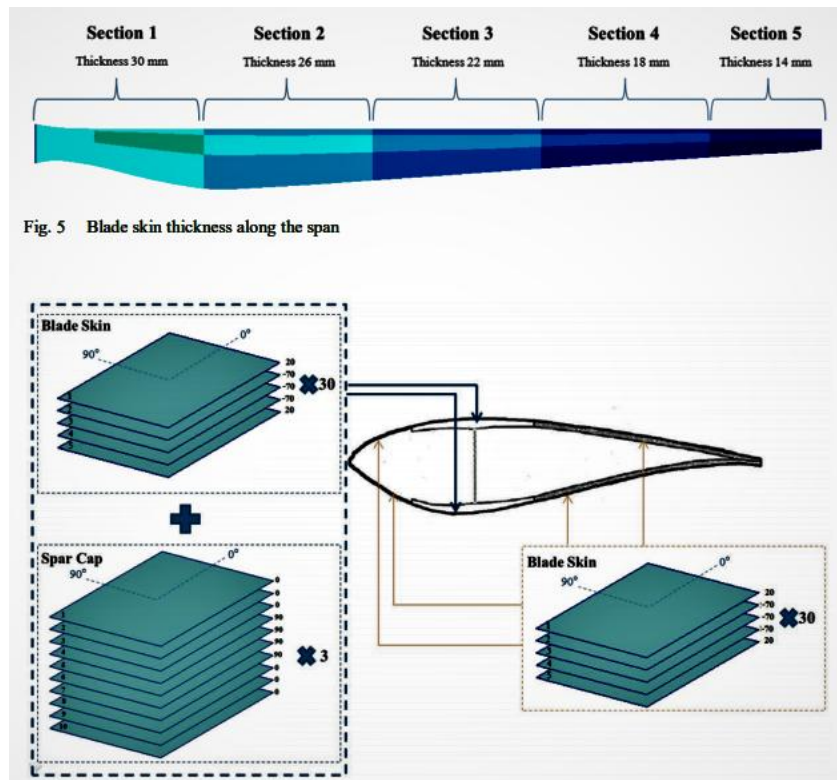


**Figure 8: Sample layup plan for a blade (Section-1 on display).** [14]

Wind turbines are modelled depending upon the engineering focus. For example; for a structural simulation rotor blades are typically modelled as cantilever beams. This procedure offers a global insight into the structural loading capability of the blade. In practice a more localized approach is undertaken and computational analysis of individual features, bonds and laminates is carried out.

### *2.1.2 FEM theoretical insight*

In engineering the material behaviour is typically described with classical continuum mechanics. This model is then applied to specific problems to get the structural mechanical behaviour. However, to solve an arbitrary problem analytical solutions are hard to obtain. Therefore, numerical methods such as “Finite element methods” (FEM) are used to solve the differential equations of the problem (typically of partial nature).

Application of mathematics & physics brings about a quantitative measure to the physical occurrences. The results are typically differential equations. Although, the exact solution to these equations for specific cases does exist. For general cases, the exact solution to these equations is unknown. However, an approximation to the exact solution is possible by application of finite element methods to the weak form of the governing differential equations. Application of finite element theory reduces the level of difficulty by bringing a differential formulation down to algebraic level. The algebraic formulation is in form of a boundary value problem and once combined with known values of function at certain points of the domain, results in the approximate solution of the problem. The method is characterized by three distinctive features:

1. The domain of the problem is characterized by a set of sub domains called “finite elements”. The set is called “mesh”.
2. Over each element the function is approximated by functions of desired type. Algebraic equations relating physical quantities across end point of the elements (called “nodes”) are developed.

3. An assembly is formed that combines results from all elements in the domain, as per continuity laws.[15]

Although, finite element methods caters various forms of non-linearity's (i.e. material, geometry and contact). We would remain restricted to linear solution space with the problem at hand.

A very important and tedious aspect of the modelling is the boundary condition and it has a considerable impact on the solution of the problem. Bad imposition of the boundary condition could result in divergence of the solution or convergence to the wrong solution. Figure shown below presents various types of boundary condition that can be applied to the domain  $\Omega$ , which is limited by boundary  $\Gamma = \partial\Omega$ . [16]

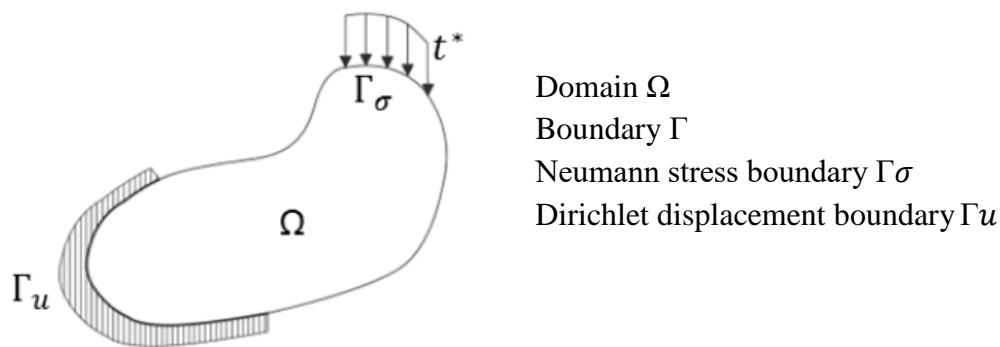


**Figure 9:Dirichlet and Neumann boundary conditions.[16]**

As presented in the work of the thesis, a change in the boundary condition would result in variation of the results.

### ***2.1.3 Solid / Volume element***

A three-dimensional(3D) solid element is the most general of all solid finite elements, as the field variables are described in all three coordinates i.e. x, y, z. It can take any form, for example (in ANSYS) it can take the shape of tetrahedron, prism or hexahedron (with flat or curved surfaces). The shape of the surface depends upon the order of “Ansatz function” and the choice of the order depends upon the geometry being modelled i.e. a higher order ansatz function would be used to model

curved geometry, for example a cylinder and a linear ansatz function would be used to model a simple geometry, for example a cube. It can be used to model any sort of structural problem at the cost of processing time and power.

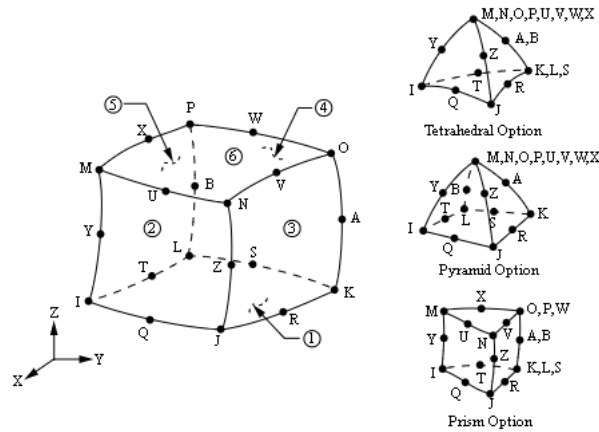


**Figure 10: SOLID186element. [17]**

Among the various restrictions concerning the element, available at the ANSYS documentation website, some important ones worth mentioning here are, Outputs of the element are available at centroid location only and some outputs are only recorded when “OUTRES” is set to “LOCP”. The element also features a layered option but it was used as a homogeneous structural solid element (KEYOPT (3) =0). [17]

We selected a solid element (“Solid 186” which is a quadratic order 20-node solid that exhibits quadratic displacement behaviour) to model the adhesives connecting the spar caps and the adhesive at the trailing edge of the blade. This selection was made to model the curvature in adhesive as dictated by the profile of the blade. Moreover, there exists “Peel stresses” (3-dimensional) within the structure where the adhesive meets the adjoining layer of composite skin and solid element would provide details of 3D-stress and deformation.

### ***2.1.4 Shell element***

Technically speaking, a solid element is the core of all elements and shell, plates etc. are all derivatives of it. Shell elements are



useful for modelling primarily thin structures, and depending upon the severity of the problem moderately thick structures (layered & layered) can also be modelled using shell elements.

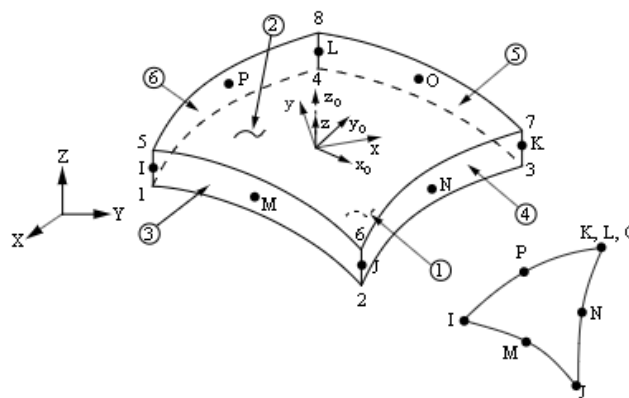


**Figure 11: Geometry of Shell 281 element. [19]**

Concerning the outputs of the shell data two commands are very important to mention here. Once the output has been written to the result file, the “LAYER” command can then be used to specify the element layer for which the data is to be processed. By default the entire element is considered to be one layer and the data that is output is from the top of the top layer and bottom of the bottom layer. Furthermore the “SHELL” command can then be used to specify the location within a layer (or element i.e. if the layer command is set/left default) for output i.e. top, mid or bottom of layer. By default ANSYS averages the values of top and bottom surface and displays the

results. The layer command can be used to overwrite the default and display or print results for various locations within a layer. Note that when using the LAYER command with “SHELL281”, “KEYOPT (8)” must be set to “2” in order to store results for all layers. Outputs of the element are available at centroid location only and some outputs are only recorded when “OUTRES” is set to “LOC1”.[19]

“Shell 281” is used to model the composite layups of the skin and the spar of the wind turbine blade as it supports modelling of composite layups. Moreover, the element is modelled based on Krichhoff assumptions, which hold for our case with good enough accuracy and the final setup is more computational efficient. .

### *2.1.5 Mass 21 element and constraint equation formulation*

ANSYS APDL has a point element that requires a single node only. The use of such an element is more like a reference point in ABAQUS users. It has six degrees of freedom, three translations and three rotations. It is useful for structural applications. The element can take mass properties in each coordinate direction; furthermore it even supports different values for translational and rotational inertias.

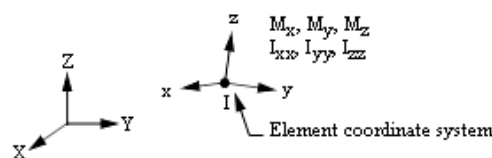


**Figure 12: Geometry of a Mass21 element.[20]**

Concerning the output from the element, the nodal displacements are included as a default nodal solution data. From the elemental solution only the reaction forces and energies could be requested as an output. In a static analysis the “Mass 21” element has no effect if there is no rotation or no acceleration or inertial relief is not turned on (“IRLF” command).[20]

As in our case we will use this element to extract nodal reactions and displacements, as inputs for our testing machine (refer to Figure-21). The “Mass-21” element will integrate in our system via constraint equations coupling it to all nodes at a specific cross section of the blade, thus depicting a perfectly rigid boundary (i.e. a load introduction).

In ANSYS APDL, various commands could be used to develop constraint equations like “CE”, “RBE3”, “CERIG”. Which one you select depends upon the problem you are handling and the scale of the problem. Please note that the constraint equations developed using commands mentioned above are for component based analysis only and do not work for assemblies in which contact based constraint equations are to be developed (see “SAS IP, Inc, Element Reference, 11.5.3.2. Tying Dissimilarly Meshed Regions Together). We develop the rigid links using the “CERIG” command. The “CERIG” command develops rigid regions, by connecting nodes (masters and slaves) via rigid links, offering one to six degree of freedoms (translational and rotational). The links can be in 2D or 3D space. The master node controls the behaviour of the slave nodes. Any translation, rotation, forces and moment enforced onto the master node is transferred to the slaves. Rotation and moments take into account the distance between the master and the slaves. In general, your slave nodes need have any degrees of freedom but your master node must have all applicable translational and rotational degrees of freedom.[20]

The following example illustrates formulation of constraint equation showing moment transfer for capability:

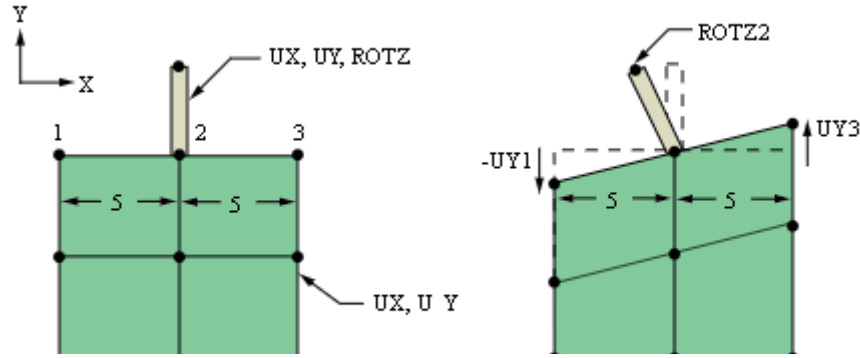


**Figure 13: Relationship between rotational and translational DOF's.[20]**

For transfer of moments between master and slave the following relation has to be typed into the command line:

$$ROTZ_2 = (UY_3 - UY_1)/10$$

The formulation of the equation is automated in ANSYS APDL and no further details about formats is required.[20] In this problem it must be documented that points “1” and “3” are closest to point “2”(the master node) in X-direction and a moment about “Z” would mean that the moment arm is calculated as per difference in X-coordinate. The rotation values, provided using the D-command, are translated to displacements with respect to the nearest nodes. This statement would further be clarified when the case of single sided loading would be discussed. A rotation applied to a master node would be translated to displacements to neighbouring nodes, according to the difference of in plane coordinates.

### ***2.1.6 Coupling degree of freedoms***

While developing or editing a model, one needs to define distinctive regions that contribute to the overall behaviour of the model such as a rigid region, pinned joints, sliding interfaces (frictionless or rough). For such special purposes elements are not predefined in software. Instead, one can associate nodal degree of freedom by using coupling constraints in the model.

When it is required that two or more degrees of freedom take on the same but unknown value they are coupled. Coupling nodes

results in formulation of constraint equations. Constraint equations have the form:

$$\text{Constant} = \sum_{I=1}^n (\text{Coefficient}(I) * U(I))$$

Where,

U (I) – Degree of freedom of term I.

N- Number of terms in the equation.

Common application of such coupling constraints are creation of a rigid body/rigid interface and tying of dissimilar meshes in model, by coupling all degree of freedoms of a set of nodes involved in the geometry of interest. [21]

Implementation of constraint equations alters the global stiffness matrix but the implementation is as such that no special numerical treatment is required for solution of equation or Eigen-analysis.[22]

### *2.1.7 Modelling with multiple meshes*

ANSYS APDL offers solutions to combine assemblies developed from orphan meshes. The ability to tie multiple meshes together can be accomplished via “CEINTF” command or via contact elements with the multipoint constraint algorithm. Another way of accomplishing the problem at hand is via the “NUMMRG” command.

“CEINTF” command connects nodes of one region to the elements of another region and writes down constraint equations for it automatically. This command ties together regions with dissimilar meshes. The inputs for the command are to be selected as per the meshed components such that at the interface location between two regions, nodes are selected from the denser mesh region (let’s call it “region-A”), and elements are selected from the sparser mesh (let’s call it “region-B”).

Once the command is executed shape functions of elements in region-B are utilized and the degrees of freedom of nodes of

region-A are interpolated according to the corresponding degrees of freedom of the nodes of elements of region-B. Constraint equations are then formulated automatically connecting nodes of both regions at the interface. ANSYS allows two tolerances for selection of nodes. Nodes which are outside the element by more than the first tolerance are not accepted as being on the interface while the nodes within the second tolerance to an element surface are moved to that surface.[20]

The second approach involves definition of a contact surface and a target surface. The contact surface must always be built on the shell element side and the target surface must always be built on the solid element side. There is no need for alignment of nodes or elements beforehand.[23]

The “NUMMRG” command could merge coincident or spatially located nodes. The node number to be assigned could be specified in the “switch” section of the command, by default the lowest node number is retained. [24]

## *2.2 Testing of wind turbines*

Testing of wind turbines is a rather difficult and costly engineering feat. Only identification and location of critical failure loads and their positions along the span of the rotor blade is a challenge itself. To add to this difficulty, length scaling of rotor comes in. [5]

Testing procedures and standards vary as per the context of testing being carried out. The testing of laminate debonding effect between layers of composites or validation of adhesive strength between spar and skin are examples of two different tests which would require two completely different approaches. Furthermore it also varies as per the observation scale of testing i.e. localized effects are being studied or global results are of concern. We would remain affixed to the global context of static testing as it would provide us with the load transfer matrix and machine loads (test bench loads).





We would further discuss static testing, of a “Smartblade 2” (serial number 1) i.e. our 20-meter rotor blade conducted at “Fraunhofer” (Bremerhaven), to explain the tediousness of the process and highlight the importance of development of a methodology to replace this engineering feat.

A total of four load cases were investigated by “Fraunhofer e.V” (Bremerhaven). The experimental procedure was identical for every loading case. Prior to testing of every case the blade had to be adjusted by rotating it about its span axis and mounting it to the test stand. For fixing the turning blocks (for loading/unloading), the appropriate positions were determined on the floor and loading cables were attached. Load cells were installed and connected to data acquisition module/measurement system. Draw wire sensors were attached to the blade via fixation to brackets (load introduction clamps) attached to the blade. Once all this was done the testing began. The load was introduced in percentages of 40, 60, 80 and 100 and upon reaching 100% the load was held for 10-seconds before unloading the blade. The displacement values obtained by the draw wire sensors were optically verified using camera placed at specific points across the testing hall.

When one test case was completed, before moving onto the next load case, the load cells and the draw wire sensors were examined to be functioning properly. For examination of load cell functionality a man hung by every load cell and his weight was recorded and verified by the monitoring system. For the check of the draw wire sensor every one of them was hand turned by a length of 1-meter and the data was recorded and verified by the monitoring system. All strain gauges and displacement sensors were reset to zero after completion of every load case. [4]

Prime Loading cases for static bend testing are depicted in table below:

**Table 3: Load cases for static testing. [4]**

	
<p><i>MYMAX-Suction side under compression</i></p>	<p><i>MYMIN-Pressure side under compression</i></p>
	
<p><i>MXMAX-Leading edge under compression</i></p>	<p><i>MXMIN-Trailing edge under compression</i></p>

As is clear that the spatial requirement to house a blade of such substantial proportions is heavy on budget. The cost of conversion of a storage room to a testing facility, setup of sensors and optical measuring equipment within the testing facility, calibration sensors, ensuring of health and safety standards, the cost to maintain a man force. With passage of time, the blades get bigger so these needs would also vary with it, and with custom designed products the chance of obsolesce are also present. Even after performing such a test, one lags data to completely verify a blade as the critical loads for every critical section along the blade span are not known. A solution is required that could scale the testing of the complete blade down to testing of various subsections of the blade such that the complete blade could be fully verified by verifying the subsections only.



## Chapter 3-Experimental and numerical setup

### 3.1 Experimental setup

The test rig/test bench assembly and its components are described. Alongside the description, all necessary data for the numerical modelling phase is also highlighted.

#### 3.1.1 Details & Specification

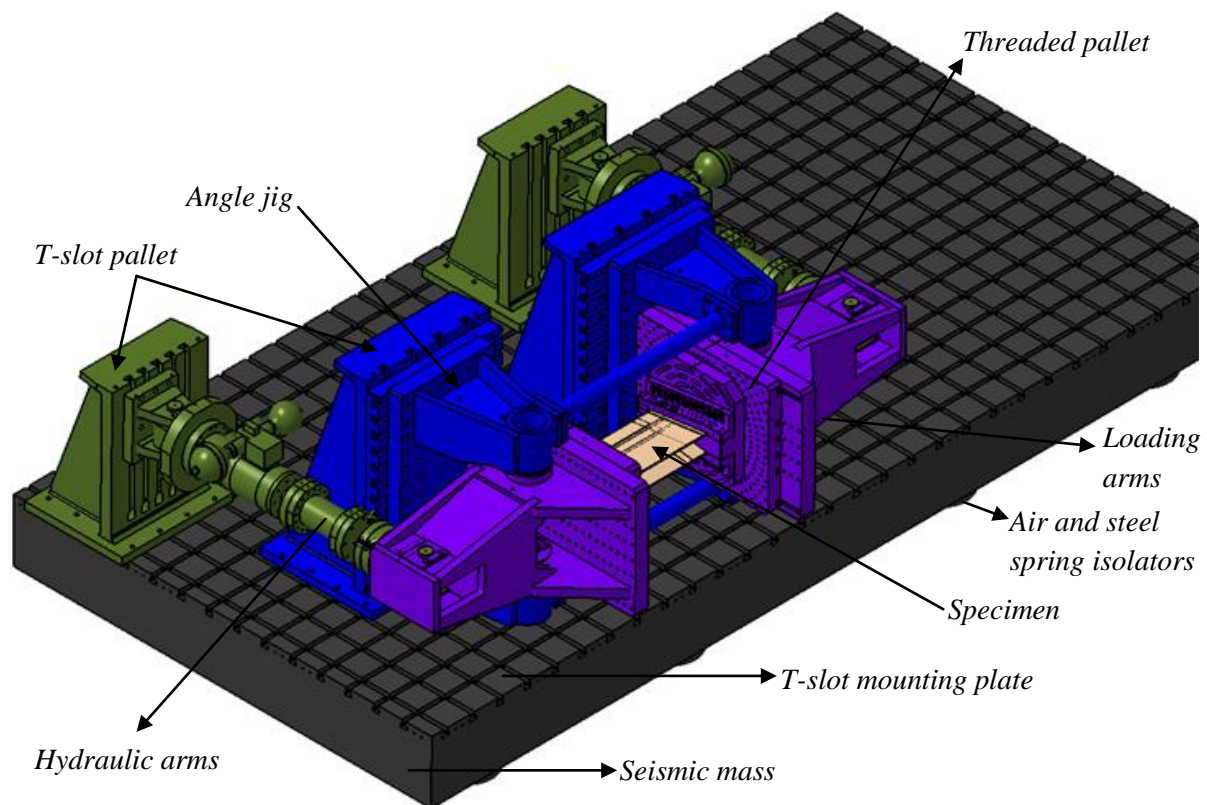


**Figure 14: CAD-Model of test bench currently present at DLR.**

A 3D-Model of the test bench is shown in the figure above. The setup has not been designed specifically for the problem at hand. The test assembly is located on a “Seismic mass” (assembly) to prevent vibration to enter the ground and damage the buildings’ infrastructure. The foundation comprises of concrete and steel spring isolators. A thick “T-slot pallet” sits

on top of the foundation connected via “anchor bolts” to the seismic mass.

Two “Hydraulic arms” mounted on two separate “T-slot pallets” placed vertically load and unload the assembly. Two “Angle jigs”, mounted on two separate “T-slot pallets”, separately hold the “loading arms” in place. The “Angle jigs” act as pivots and convert the horizontal force applied by “hydraulic arms” to moments which are then applied to the subsection via loading arms. Within the assembly, midway between the pump and loading arm is a load cell that measures the transferred load to the angle jigs.

Technical details about components which would further be useful in modelling the test bench are given in table below:

**Table 4: Technical specifications of hydraulic cylinders.**

Total Stroke length of hydraulics	100mm
Available Stroke length of hydraulics	+/- 50mm

A picture of the actual setup in the testing laboratory of “Department of lightweight construction and adaptronics” at “DLR” (Braunschweig) is given below:

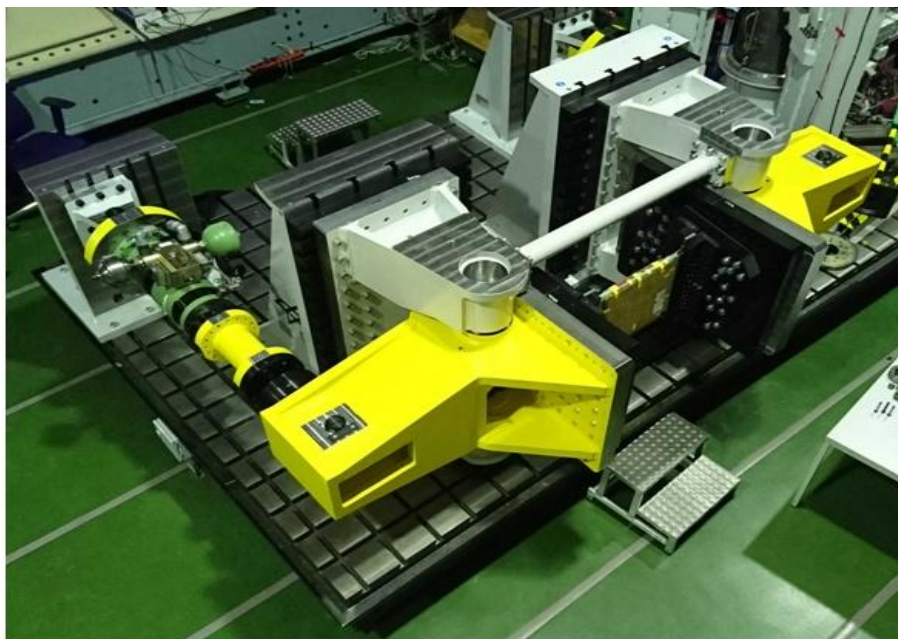


**Figure 15: Test bench currently present at DLR.**

### 3.1.2 Loading capability

The test rig was not designed for the purpose of testing subsections of wind turbine blades but is being used to validate certain small regions of the blades for example; a small section of the trailing edge can be tested to study bond strength. The goal is to figure out that to what extent we can achieve a replica of the stress state within the subsection (specimen) as in the actual blade, using this test rig. This replicated stress state has to be generated using some combination of loads, possible via the test bench. Ideally speaking, it seems that the replication of stress along the X-axis is possible considering the spectrum of load cases possible on test rig.

Referring back to “Figure-2”, one observes that including the movement of specimen within the periphery of the loading arm i.e. adding eccentricity between neutral axis of the subsection and the centre coordinate of loading arms(epicentre of load introduction), provides us with the possibility of extending the set of possible load cases. Refer to figure below:

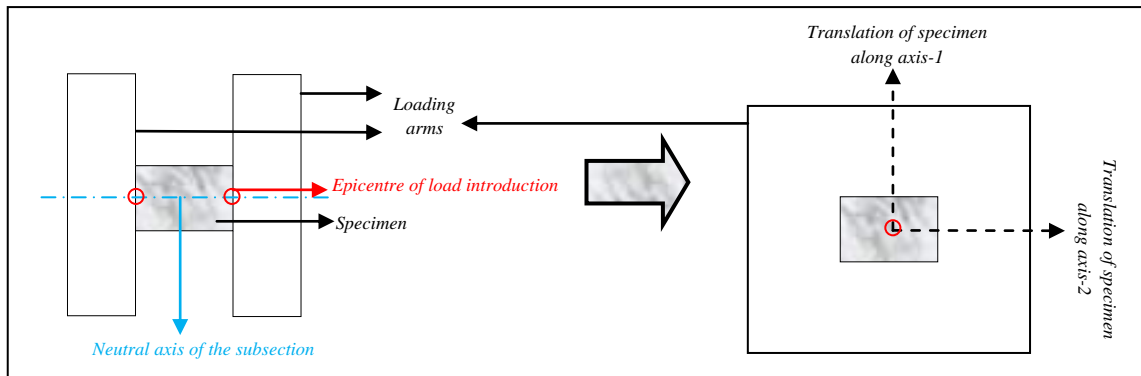


**Figure 16: Extension of possible load set via translation of specimen.**

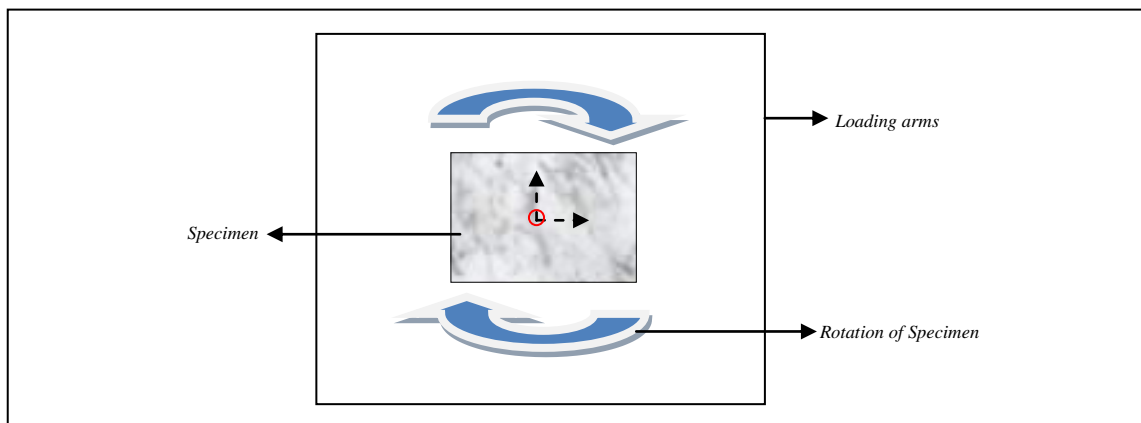


**Figure 17: Extension of possible load set via rotation of specimen.**

Another methodology of extending our set of possible load cases is by altering the orientation of the subsection in the loading arms. Refer to figure above for further clarification.

### 3.2 Numerical setup

The wind turbine blade was modelled in ABAQUS and exported as an orphan mesh. The model comprises of shell and volume (solid) elements. The adhesive is modelled with quadratic serendipity volume element and the thin walled structure is modelled using quadratic serendipity shell element. The stacking sequence is defined as per the layup plan of the actual wind turbine blade and the material models of elements utilize “Laminate theory”.

The fibre and matrix are not separately modelled. The layers are treated as a homogeneous material with transversal isotropic material symmetry. Balsa wood is used as sandwich core has isotropic material symmetry.

The numerical approach to implement the stress replication process using the test rig, in finite element framework is described. The script was implemented in ANSYS APDL. In this model the complete testing cycle was simulated. All data relevant to the inputs is highlighted in table below:

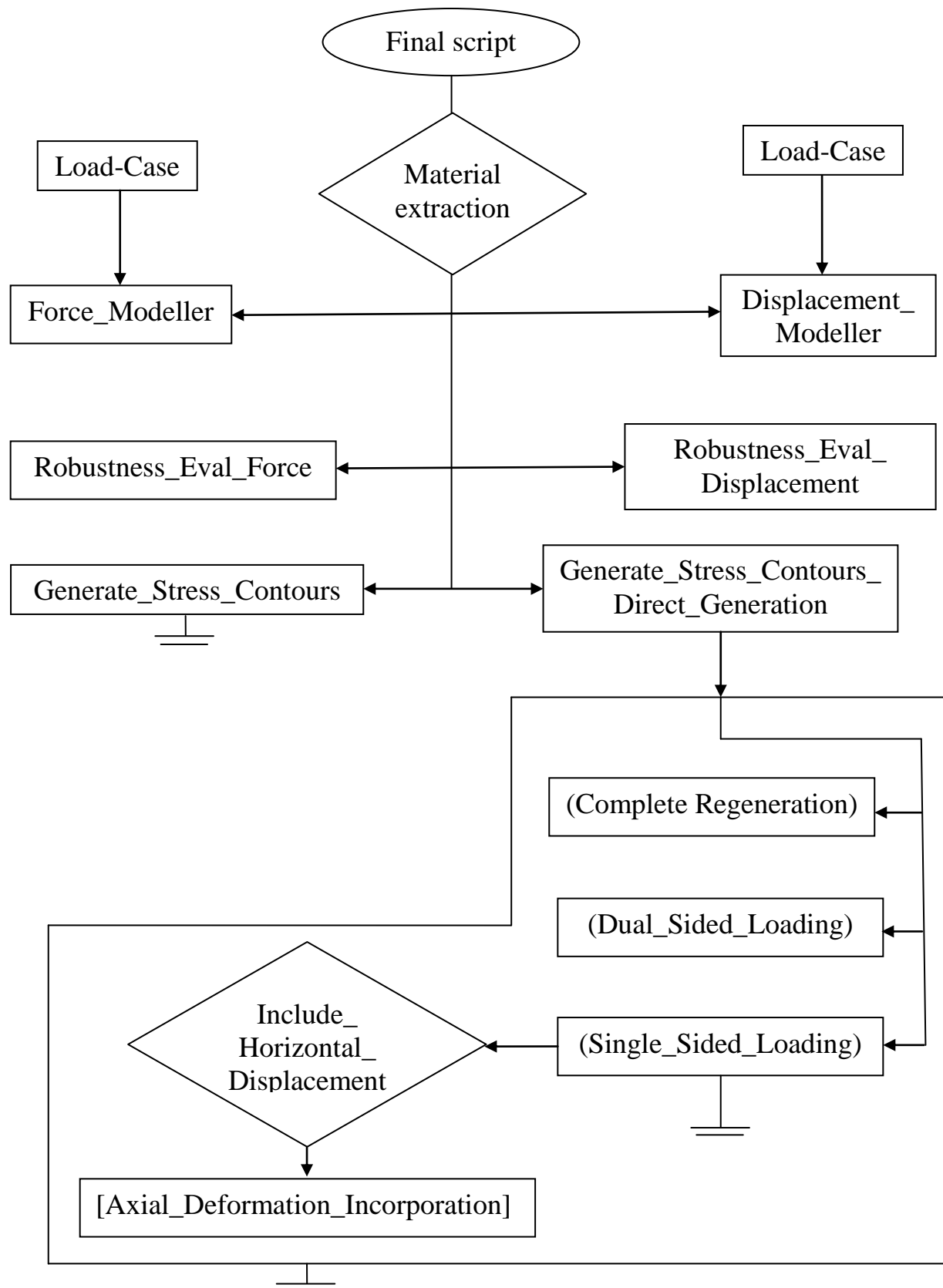
**Table 5: Inputs for the model.**

FORCE_CONTROLLED	Module selection (Force/displacement)
ROB_TEST	
MODEL_LOADING_ARMS	
GSC=0	
MAX_LENGTH	Blade section parameters
CUTOUT_LOC_1	
CUTOUT_LOC_2	
FARTHEST_POINT_X	
ROB_TEST_OFFSET_1	Robustness test parameters
ROB_TEST_OFFSET_2	
ROB_COUNTER	
PALLET_THICKNESS	Parameters for loading arm modeller
DIMENSIONS_OF_LOADING_ARM	
ROT_VALUE_TEMP	

SENSOR_LOC_X	Sensor location details
SENSOR_LOC_Y	
SENSOR_LOC_Z	
TRANS_X_CO1	Inputs for module “Generate stress contours”
TRANS_Y_CO1	
TRANS_Z_CO1	
ROT_X_CO1	
ROT_Y_CO1	
ROT_Z_CO1	
TRANS_X_CO2	
TRANS_Y_CO2	
TRANS_Z_CO2	
ROT_X_CO2	
STRT_ROT_Y	
MAX_ROT_Y	
INC_ROT_Y	
STRT_ROT_Z	
MAX_ROT_Z	
INC_ROT_Z	
BLADE_ANGLE	
STRT_Y	
STRT_Z	
INC_Y	
INC_Z	
MAX_Y_GSC	
MAX_Z_GSC	
GSC_2=1	Inputs for the “Direct generation method”
MAX_LENGTH	
MIN_SPECIMEN_SIZE	
MAX_SPECIMEN_SIZE	
JUMP_IN_SPECIMEN_SIZE	

The detailing of each class i.e. the transfer variables and outputs were decided as the script was being developed. At the final stages of the thesis the classes were properly interlinked and automated to maximum extent possible. The classes which were kept out of the automation loop were kept so because of absence of a feedback variable, required from the software, for automation purposes. The “building block method” was employed to ease customization and alteration of the developed program. The various classes of the program output to different

text files. A flow diagram of classes (kept within the automation loop) has been sketched out below:



In the flow diagrams the classes that could not be automated were not drawn but are discussed ahead in the thesis and it is mentioned in their respective sections that they are not sketched out in the flow diagram. For details concerning “Text files” (output files) of various classes, refer to the table below:

**Table 6: Model classes and respective outputs.**

<b>Class name</b>	<b>Output file generated</b>
Force_Modeller	MATRIX_ENTRIES
Displacement_Modeller	MATRIX_ENTRIES
Robustness_Eval_Force	ROBUSTNESS_TEST_FORCE_OUTPUT
Robustness_Eval_Displacement	ROBUSTNESS_TEST_DISPLACEMENT_OUTPUT
Generate_Stress_Contours	DATA_FOR_S
Complete Regeneration	SPECIMEN_COMPLETE_STRESS_STATE
Dual_Sided_Loading	SPECIMEN_DUAL_SIDED_APPROACH_DIFFERENT_YZWOD
Single_Sided_Loading	SPECIMEN_SINGLE_SIDED_APPROACH_DIFFERENT_YZWOD
Axial_Deformation_Incorporation	REPLICATED_SST

The class titled “Generate\_Stress\_Contours\_Direct\_Generation” writes two output files, out of which one depends upon which method you select to replicate the stress state of the complete blade i.e. “Dual\_Sided\_Loading”, “Single\_Sided\_Loading” or “Single\_Sided\_Loading”. The other output file generated is “CBT” which has details of stress state from the complete blade in it.

For “Single\_Sided\_Loading(Axial\_Deformation\_Incorporation)” the output file containing details of the stress state from the complete blade is titled “ACTUAL\_SST”. The other output file is mentioned in the table above.

### ***3.2.1 Model description***

The aerodynamic hull section was the starting point of model development. All section including spar, spar caps, adhesive bonds etc. Including the material definitions were created and

defined in ABAQUS. The final mesh was transformed into input data for finite element tools (ANSYS, NASTRAN etc).

Three material classes are used to develop the blade, namely:

- 1) Glass fiber reinforced plastics for the skin.
- 2) Foam material for sandwich stiffened regions.
- 3) Adhesive material to glue the parts of the blade.

A material whose young modulus is 10 N/mm<sup>2</sup> is a pseudo material (artificial material) used to catch stress concentrations at various locations of the blade & for group selection purposes. A table containing material details as they are defined in the software has been attached in the appendix. For selection and amendment purposes, kindly refer to the appendix.

The thin walled structures are modelled with serendipity quadratic finite shell elements. The use of shell elements enabled the usage of stacking which defined the layups. The stacking directions are shown below:

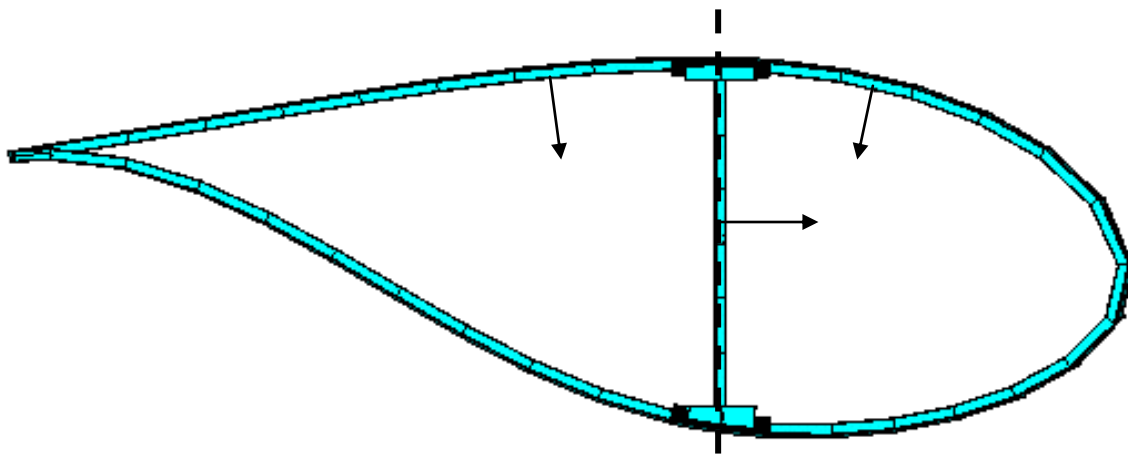


**Figure 18: Reference plane and stacking direction.**

It is important, to highlight certain differences between the actual rotor blade and the finite element model of the rotor blade. At the trailing edge there is no sandwich free region in the finite element model which would result in higher bending stiffness at the trailing edge. Numerical analysis of the trailing



edge would output results that would be overestimated, Also the local strain measurement would be affected but as the tensile stiffness of the extra foam is very small the global results will not be severely affected. The adhesives are thicker in the model compared to the actual blade resulting in stiffer response to local loads. At the leading edge the adhesive section has not been modelled as it is very thin. The tip has not been modelled as a varying cross section makes the meshing process very cumbersome. No “Bolts” and “Profile altering actuators” have been modelled. During production the root was built separately and glued to the rest of the blade, but this adhesive joint was not modelled. All these steps were taken to reduce the complexity in the model, but would affect the results locally but the global results would remain the same (More or less).

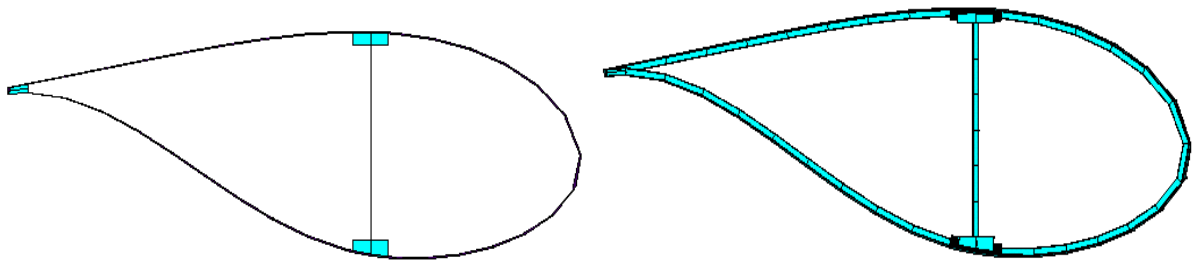


**Figure 19: Solid and shell distribution.**

There is an overlap between shell and volume elements as indicated by the figure above. The model was prepared with the goal to publish the model, after validation. The geometry of the blade, from which a section was to be sliced out and numerically analyzed, was provided in form of an orphan mesh. The span of the blade is 20-meter (20000millimeters) and chord length is 2.39-meter (2399millimeters). In our discussion, we would remain restricted to section between 12.5-meters to 16-meters of the blade. Details of materials used for modelling the blade are mentioned below:

**Table 7: Materials used in modelling the 20meter specimen.**

Material	Orientation	E <sub>1</sub> (MPa)	E <sub>2</sub> (MPa)	G <sub>12</sub> (MPa)	$\nu_{12}$	P (kg/m <sup>3</sup> )	h (mm)
UD	0°	44151	14526	3699	0.3	1948	0.827
2AX45	±45°	11316	11316	11978	0.633	1875	0.625
2AX45manual layup	±45°	8802	8802	8608	0.601	1658	0.892
2AX90	0° / 90°	26430	27520	3464	0.124	1875	0.651
3AX	0° / ±45°	29873	13377	6918	0.466	1875	0.922
3AX manual layup	0° / ±45°	21888	9473	5126	0.46	1658	1.318
Balsa Baltek SB.100	-	35	35	105	0.3	291	tbid
Foam Airex C70- 55-20mm-spar	-	55	55	22	0.3	180	20
Foam Airex C70- 55-20mm	-	55	55	22	0.3	279	20
Foam Airex C70- 55-15mm	-	55	55	22	0.3	314	15
Foam Airex C70- 55-10mm	-	55	55	22	0.3	384	10
Foam Airex C70- 55-5mm	-	55	55	22	0.3	596	5
ADH/HARDENER	-	4864	4864	1828	0.33		1160
Pseudo material	-	10	10	3.84	0.3	1.0e-5	0.1

**Table 8: Material numbers/labels in ANSYS APDL.**

UD	7
2AX45	22
2AX90	24
3AX	18
3AX manual layup	4
Balsa Baltek SB.100	12
Foam Airex C70-55-20mm-spar	32
Foam Airex C70-55-20mm	37
Foam Airex C70-55-15mm	25
Foam Airex C70-55-10mm	19
Foam Airex C70-55-5mm	13
ADH/HARDENER	23

Geometry of the model is as such that, the X-axis is parallel to the span of the blade, Y-axis is parallel to thickness and the Z-axis is parallel to the chord of the blade. For a better understanding of the coordinate system, kindly refer to the figure below:

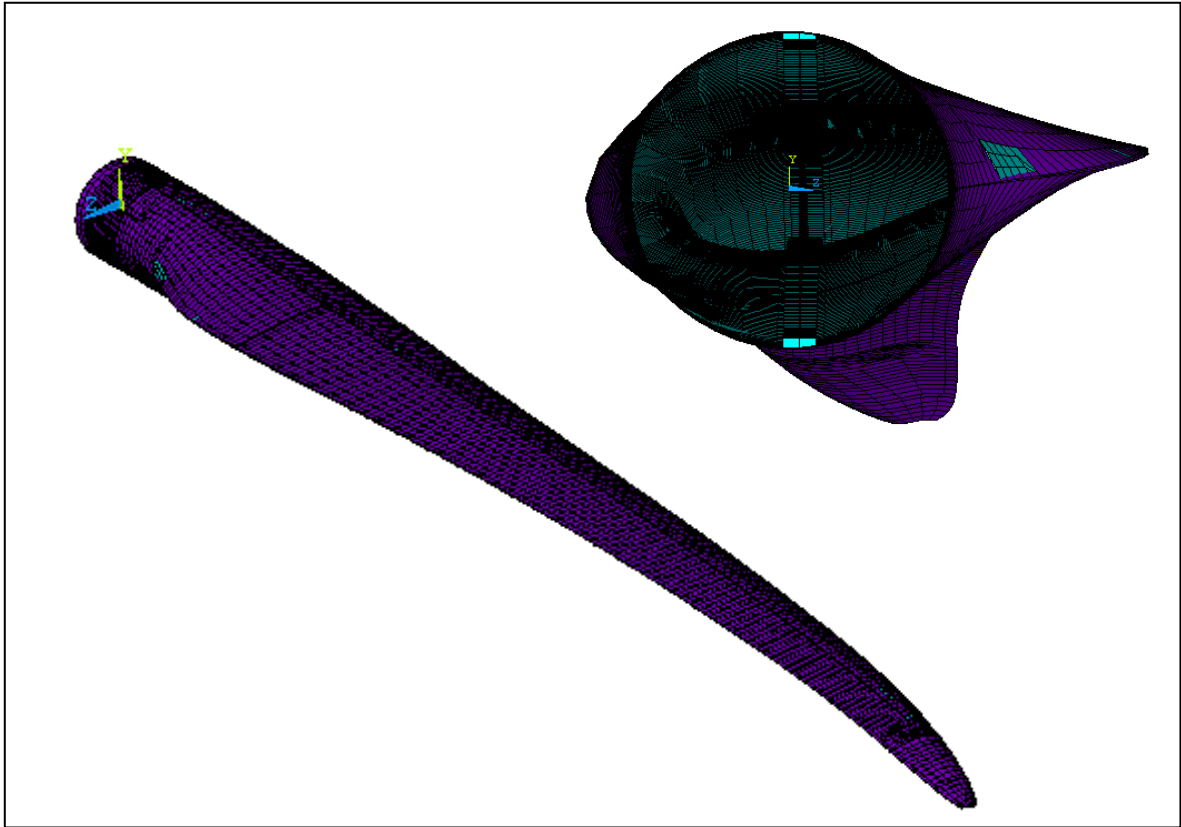


**Figure 20: Coordinate system of blade.**

### *3.2.2 Transfer matrix extraction*

At the two cut out locations provided in input (X-Coordinate demanded by the user only), two master nodes are generated. The “Mass-21” element is associated with these master nodes. Then each individual element is connected to the neighbouring nodes (slave nodes) in the YZ-Plane. All degree of freedoms of the slaves’ are coupled to the master node. Such complete coupling results in creation of a rigid surface (i.e. the load introduction in the test bench).

The slave nodes take upon the translations and rotations as dictated by the master node. Similarly, the collective response of the slave nodes is registered at the master node. This collective response generated at master node will provide us the inputs for our test bench (be it force or displacements).

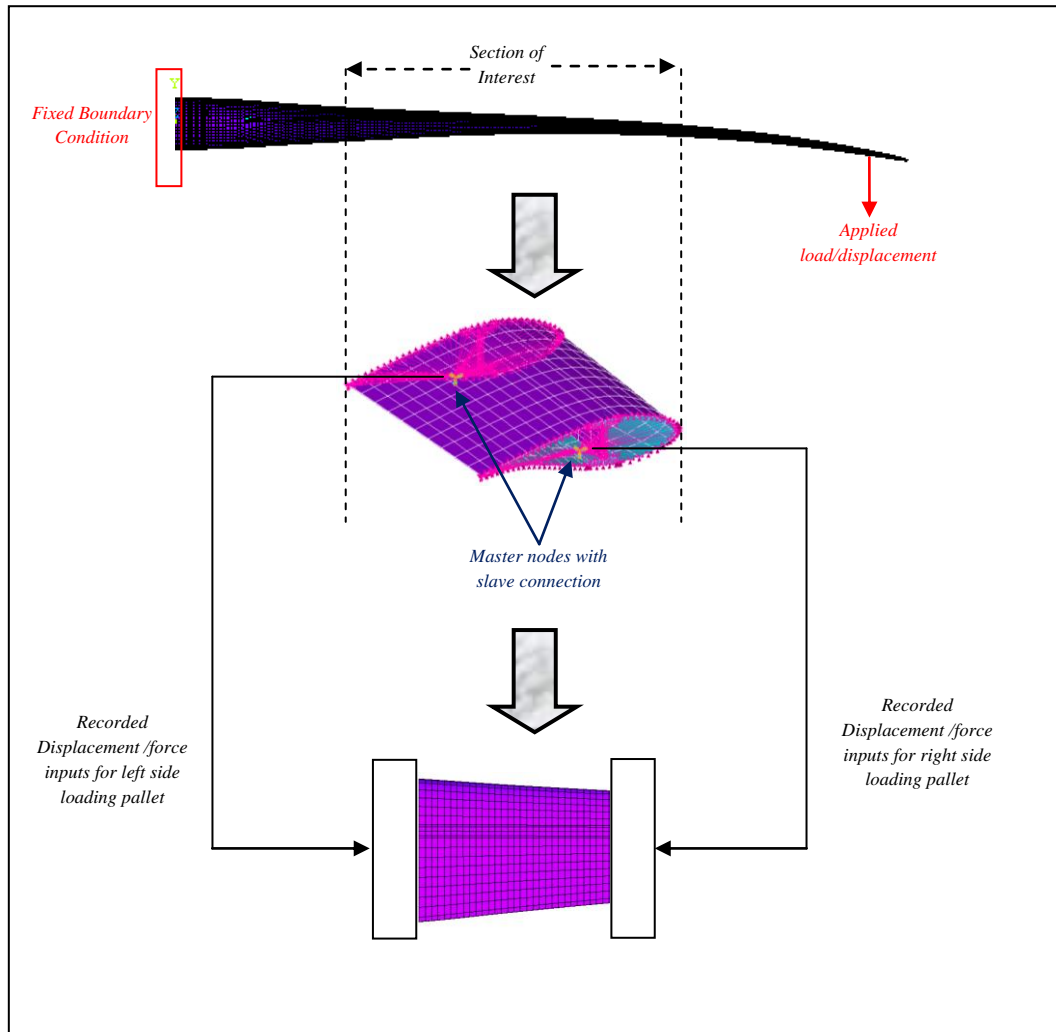


**Figure 21: Transfer matrix & machine load extraction**  
**(refer to fig. 16 & 17).**

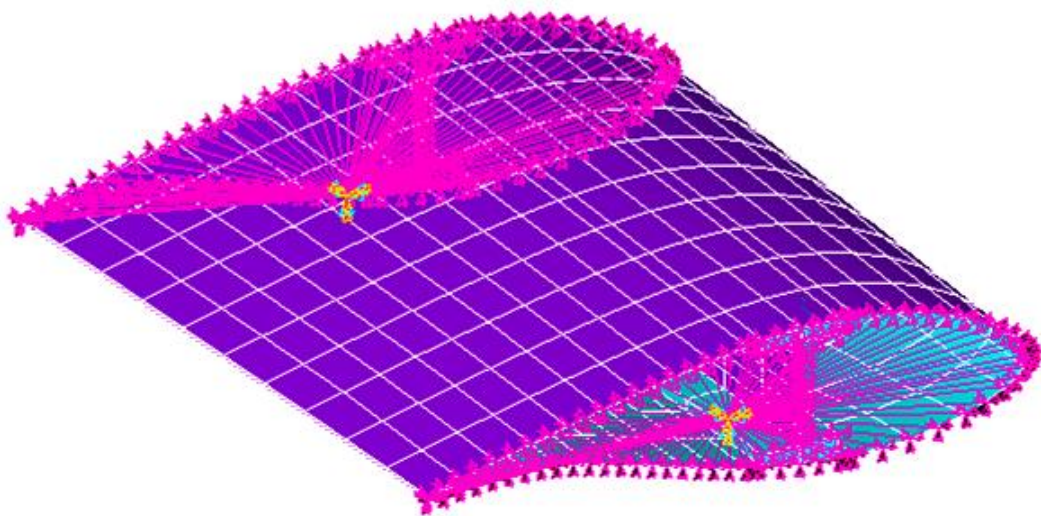


**Figure 22: Rigid constraints between master and slave nodes.**

### *3.2.3 Implementation of boundary condition*

There exist two concepts of implementation of boundary condition, to achieve replication of the desired stress state, from the full blade model. They are as follow:

1. Application of a rotation/displacement at master nodes of the subsection. This would make use of a “Dirichlet boundary condition” at the boundary of our domain. Later on the boundary condition could be varied, subject to various constraints, until desired results are achieved.
2. Search for a point of zero reaction force within the specimen and apply a fixed boundary condition (Dirichlet boundary condition) there. Then apply forces/moment to the master nodes of the specimen and observe response. This would make use of a “Neumann boundary condition” at the boundary of our domain. This case is subject to case of availability of a traction free position, within the subsection. Even if the condition of zero traction is satisfied the effect of a fixed boundary condition would affect the results in its vicinity. As “Saint-Venant principle” dictates, the effects of loading dissipate as distance from the point of application of load increases.[25] This signifies that the point where a boundary condition is applied should be at a considerable distance apart from the point of interest (i.e. the point where the stress state is being monitored).

Given, the above discussion it was decided to proceed on with the first option as implementation of “Neumann Boundary condition” would be very flawed even when possible to implement.

## Chapter 4-Results

### *4.1 Transfer Matrix*

#### *4.1.1 Reaction loads/Resulting deformation to transfer matrix*

For transfer matrix formulation we need the reaction loads generated in response to a load/displacement applied to a location on the blade. We have a set of 6-possible unit load cases, comprising of three forces and three moments. Reactions generated for every load case are to be observed and recorded in a matrix.

For force controlled test, all degrees of freedom at the master node are restricted. A unit load case is applied at any desired coordinate of the blade. The reaction forces generated at the fixed master node, dictate the reaction force vector. Upon looping through all load cases (unit) and combining the reaction force vectors column wise gives us our transfer matrix for force controlled test.

For a displacement controlled test, the transfer matrix formulation is different in the fact that a fully constrained boundary condition is applied to the root of the blade. A unit displacement/rotation is applied at the desired coordinate of the blade and the resulting deformation that occurs at the master node is recorded (which is the deformation of the cross section). This gives us the deformation vector for the cross section. Upon looping through all load cases (displacement/rotations) and combining the cross section deformation vectors column wise gives us our transfer matrix for displacement controlled test. (.)

Transfer matrices take us from the global to the local loads and the inverse of this matrix retrace back from the local to the global loads. The reaction loads/resulting deformations are written down in a separate file titled “NODAL-REACTIONS”, before being transferred to the main output file. Some additional transfer matrices generated using the script developed are given in the appendix

```

**RUN START**

TEST TYPE: DISPLACEMENT CONTROLLED

ROOT CENTER IS GLOBAL ZERO
GENERATING MATRIX FOR X (mm): 12500.00
NUMBER OF NODES SELECTED ARE:- 88.00

MASTER NODE AT:
X (mm): 12500.00
Y (mm): -117.68
Z (mm): 250.16

LOADING POINT DETAILS:
FORCE AT X (mm): 18000.00
FORCE AT Y (mm): -551.80
FORCE AT Z (mm): 123.09

-DISTANCE BETWEEN MASTER AND LOAD IN X-DIRECTION: 5500.00
-DISTANCE BETWEEN MASTER AND LOAD IN Y-DIRECTION: -434.12
-DISTANCE BETWEEN MASTER AND LOAD IN Z-DIRECTION: -127.07

TRANSFER MATRICES:
MATRIX OF TRANSFORMATION (GLOBAL TO LOCAL)
0.14031E+00 -0.33193E-02 -0.10206E-01 0.65671E-03 0.72378E-03 0.13719E-01
-0.27421E+01 0.47842E+00 0.53343E-02 -0.42499E-02 -0.14530E-01 -0.25984E+00
0.92963E-02 0.92640E-02 0.44072E+00 -0.24877E-01 0.46703E-02 0.26868E-02
0.97792E-04 -0.12776E-04 -0.52777E-04 0.80357E-04 -0.13462E-04 0.16983E-04
-0.25024E-04 0.28200E-05 -0.74155E-04 0.14521E-05 -0.42499E-06 -0.27098E-05
-0.28152E-03 0.91259E-04 -0.28779E-05 0.45342E-05 -0.21072E-05 -0.23077E-04

INVERSE MATRIX IS (LOCAL TO GLOBAL)
0.43746E+02 0.55134E+01 -0.47921E+02 -0.89357E+04 -0.28350E+06 -0.14939E+05
-0.17454E+03 -0.12869E+02 -0.22921E+03 -0.53847E+05 -0.13058E+07 0.12815E+06
0.83615E+00 0.39445E+00 -0.33097E+01 -0.37370E+03 -0.32948E+05 -0.73569E+03
0.26204E+05 0.18891E+04 0.24995E+05 0.59281E+07 0.14144E+09 -0.15028E+08
0.14513E+06 0.10443E+05 0.13887E+06 0.32853E+08 0.78597E+09 -0.83253E+08
-0.93272E+04 -0.70059E+03 -0.80909E+04 -0.19390E+07 -0.45679E+08 0.52950E+07

```

**Figure 23: Transfer matrices for a displacement controlled test.**

A sample transfer matrix is given above. The results depicted in the figure are for a displacement controlled test with fixation at “X-coordinate” of “12500”. The “Y” and the “Z” coordinate are determined atomically by the script. The details of the loading point are also summarized in the output file.

Some common anomalies worth mentioning here are:

- 1) The program crashes when the node selection process takes more than 20-iterations.
- 2) At some points across the span of the blade, the number of nodes selected to be connected to the master node is less than five. This effect is very prominent at the point where the circular section of the root ends and the spar section begins for example at “X-coordinate” of “1000” the number of nodes selected is “0”.

The solutions to both the problems are the same i.e. to adjust the node selection tolerance in the main file (titled “Final Script”).

#### *4.1.2 Matrix Robustness test*

The Matrix generation algorithms were tested for robustness. The location of the master node was varied in the YZ-plane and the deformed state of the blade was monitored. As the position of the master node is varied (in YZ-Plane), the reaction force vectors should alter themselves automatically, but the resulting deformed state of the blade must not change as the resulting displacements produced by the resulting force/deformation vectors is the same.

A common observation node was selected, located at the centre of the subsection. For both force controlled and displacement controlled test, the position of master node at “Cutout location-2” was varied and loaded. The loading for both cases was defined by a column entry of the transfer matrix (global to local). In our transfer matrices each column represents a unique set of reactions for a unique load cases.

For the transfer matrix algorithm of the force controlled test, all nodes at “Cutout location-1” were fixed. For the transfer matrix algorithm of displacement controlled test, all nodes at all root nodes were fixed. It must be mentioned here that the problem being dealt with is a linear problem and thus the forces have been amplified by a factor of “100000” to output a better comprehensible result for discussion, although this is mere a scaling factor and has nothing to do with the authenticity of the results. The control for the amplification factor (titled: “D\_MULT” and “D\_MULT”), the control of variation in the “Y” and “Z” coordinates (titled: “Y\_SHIFT” AND “Z\_SHIFT”) and the loop parameter for control of the evaluation run (titled: “ROB\_COUNTER”) are placed within the files titled “Robustness\_Eval\_DISPLACEMENT” and “Robustness\_Eval\_FORCE” for future amendments.

This exercise also highlighted the importance of positioning of master node when applying a fully constrained condition to it. Any recorded reaction moment strongly depended on the offset



between the coordinates of the loading point and of the mater node.

The results for two different and both different types of tests, with all necessary details are displayed below. For further clarification of unique load cases refer to the appendix. In the appendix, results for all 6 unique, unit load cases, have been shared for both force and displacement controlled tests with variations for “Y” and “Z” coordinates (75mm in each coordinate).The replication of deformation state was achieved for all load cases by 100%. So, it is proven that variation of location of master node in planar coordinates, and a change in the unique load case alter the transfer matrices and replicates the deformation state by 100% (theoretically). This was what was expected as the outcome from the algorithm robustness test and was achieved.

```

**ROBUSTNESS TEST START**
TYPE: FORCE CONTROLLED
(FIXED AT CUTOUT LOCATION-1)
(MASS ELEMENT AT CUTOUT_LOC_2 WI BE THE LOADING POINT)

LOCATION OF MASS ELEMENT:
NODE NUMBER      33524.00
X_COORDINATE     16000.00
Y_COORDINATE     -377.80
Z_COORDINATE      215.32

NODE UNDER OBSERVATION: 24033.00

NODAL DISPLACEMENTS(mm):
      UX      UY      UZ
-0.58219E+00 -0.11459E+02  0.98362E+00

**ROBUSTNESS TEST END**

**ROBUSTNESS TEST START**
TYPE: FORCE CONTROLLED
(FIXED AT CUTOUT LOCATION-1)
(MASS ELEMENT AT CUTOUT_LOC_2 WI BE THE LOADING POINT)

LOCATION OF MASS ELEMENT:
NODE NUMBER      33524.00
X_COORDINATE     16000.00
Y_COORDINATE     -277.80
Z_COORDINATE      315.32

NODE UNDER OBSERVATION: 24033.00

NODAL DISPLACEMENTS(mm):
      UX      UY      UZ
-0.58219E+00 -0.11459E+02  0.98362E+00

**ROBUSTNESS TEST END**

```

**Figure 24: Robustness test output (Test type: Force controlled, variation along Y-axis: 100 mm, variation along Z-axis: 100 mm).**

```

**ROBUSTNESS TESTRUN START**
TYPE: DISPLACEMENT CONTROLLED
(ALL ROOT NODES ARE FIXED)
(MASS ELEMENT AT CUTOUT_LOC_2 WI BE THE LOADING POINT)

LOCATION OF MASS ELEMENT:
NODE NUMBER      33524.00
X_COORDINATE     16000.00
Y_COORDINATE     -377.80
Z_COORDINATE      215.32

NODE UNDER OBSERVATION: 24033.00

STRUCTURAL DISPLACEMENTS ARE:
      UX      UY      UZ
0.14155E+01 -0.25380E+02  0.27966E+00

**ROBUSTNESS TESTRUN END**

**ROBUSTNESS TESTRUN START**
TYPE: DISPLACEMENT CONTROLLED
(ALL ROOT NODES ARE FIXED)
(MASS ELEMENT AT CUTOUT_LOC_2 WI BE THE LOADING POINT)

LOCATION OF MASS ELEMENT:
NODE NUMBER      33526.00
X_COORDINATE     16000.00
Y_COORDINATE     -302.80
Z_COORDINATE      290.32

NODE UNDER OBSERVATION: 24033.00

STRUCTURAL DISPLACEMENTS ARE:
      UX      UY      UZ
0.14155E+01 -0.25380E+02  0.27966E+00

**ROBUSTNESS TESTRUN END**

```

**Figure 25: Robustness test output (Test type: Displacement controlled, variation along Y-axis: 100 mm, variation along Z-axis: 100 mm).**

## 4.2 Boundary condition verification

### 4.2.1 Threaded pallets modelling

The need of modelling the “threaded pallets” (load introduction) into the system was a question that arose when the sensor placement was discussed. The outcome was to see if the pallets were rigid enough so that the sensors could be attached to the side opposite to where the subsection was attached. In case the pallet underwent extensive straining, a heat treatment would be required to increase hardness.

A module (titled: “LOADING\_PALLET-RIGIDITY”) was developed for this purpose. Unfortunately, due to lack of a feedback parameter by the program to check and alter the

meshing parameter, this task was kept out of the script automation cycle, as it required repeated hit and try to achieve a suitable merger between the two independent meshes (the threaded pallet and the blade). This class has not been sketched out in the flow diagram.

There are a total of two outcomes from this module of the programme. One outcome is an element table (titled: “LOADING\_PALLET\_OUTPUT”) comprising of details of strains of the elements nearest to the attachment interface. The element table automatically highlights the maximum and minimum values of strains with element numbers.

Another outcome of the module is a text file (titled: “LOADING\_PALLET\_NODAL\_OUTPUT”), comprising of details of nodal deformation of nodes at the interface. This file can be processed in python to plot node number versus deformation plot. This plot would give information of nodes that have successfully merged and also an idea of the rigidity of the pallet. A section of the element table from one attempt (at X-coordinate of 2200) is depicted below, with all details:

```

**MESHING DETAILS**
MERGING NODES AT LOCATION:
0.22000E+04
NO OF NODES TO MERGE:
0.10600E+03
ELEMENT SIZE AT AREA OF MERGE INTERFACE:
0.80000E+02
ELEMENT SIZE FOR REMAINING AREAS:
0.80000E+02
MERGING TOLERANCE:
0.50000E-01

PRINT ELEMENT TABLE ITEMS PER ELEMENT

***** POST1 ELEMENT TABLE LISTING *****

```

STAT ELEM	CURRENT STX	CURRENT STY	CURRENT STZ	CURRENT STXY	CURRENT STYZ	CURRENT STXZ
14398	0.62517E-05	0.15632E-04	0.89766E-06	0.54470E-05	0.99349E-05	0.96284E-06
14413	0.46041E-05	0.12130E-04	0.12142E-05	0.51807E-05	0.32131E-05	0.10915E-05
14417	0.61171E-05	0.15642E-04	0.13385E-05	0.19019E-05	0.96629E-05	0.30564E-06
14462	0.57536E-05	0.14499E-04	0.10513E-05	0.18468E-05	0.64890E-05	0.34593E-06
14478	0.42934E-05	0.11949E-04	0.17235E-05	0.78079E-05	0.46958E-05	0.16267E-05
15079	0.12146E-05	0.63726E-05	0.35045E-05	0.33988E-05	0.39746E-06	0.98545E-06
15081	0.11282E-05	0.70932E-05	0.42841E-05	0.84743E-05	0.39608E-06	0.25098E-05
15619	0.21835E-06	0.34088E-05	0.28870E-05	0.32257E-05	0.20721E-06	0.10789E-05
15652	0.21896E-05	0.45116E-06	0.46962E-05	0.14863E-05	0.31938E-05	0.76307E-06
16254	0.10198E-04	0.90232E-05	0.35089E-04	0.42150E-05	0.10065E-04	0.18925E-04
16483	0.41134E-06	0.58181E-05	0.48611E-05	0.16294E-05	0.14666E-06	0.59439E-06
16753	0.10789E-05	0.14716E-05	0.40743E-05	0.59907E-05	0.18516E-05	0.26357E-05
16756	0.23950E-06	0.34133E-05	0.39786E-05	0.31885E-05	0.74761E-06	0.12429E-05
16851	0.28996E-05	0.10317E-04	0.34519E-05	0.48853E-05	0.31763E-05	0.14249E-05
16917	0.16877E-05	0.79283E-05	0.39763E-05	0.18239E-05	0.39269E-06	0.48286E-06
16932	0.90052E-06	0.51712E-05	0.30514E-05	0.16528E-05	0.26253E-06	0.50922E-06
16942	0.23185E-05	0.23271E-05	0.30773E-05	0.15512E-05	0.26286E-05	0.70132E-06
16960	0.13711E-06	0.11535E-04	0.11197E-04	0.19086E-05	0.23104E-05	0.10784E-05
17079	0.70071E-06	0.18531E-04	0.17110E-04	0.15320E-05	0.20856E-06	0.14887E-05
17084	0.19394E-05	0.21586E-05	0.23674E-05	0.15764E-05	0.19733E-05	0.64432E-06
17186	0.41380E-05	0.10578E-04	0.98423E-06	0.69373E-06	0.13945E-04	0.46738E-06
17272	0.63881E-05	0.35520E-04	0.51517E-04	0.66312E-05	0.67846E-04	0.73644E-05

**Figure 26: Element table output for threaded pallet deformation.**

## *4.3 Stress state replication*

We now have the tools necessary to take us down from the global level to the local level and vice versa if needed. Now what we need is a set of inputs for our machine. Two methods have been discussed below in this section. Their advantages and disadvantages have also been listed ahead.

### *4.3.1 Direct generation method*

The “Direct generation method”, is an approach that utilizes the kinematics of the problem at hand to achieve replication of the stress state. We extract the deformation data from the numerical analysis of the complete blade and use it as inputs for our machine's actuators.

In numerical aspects, the file titled “GENERATE\_STRESS\_CONTOURS\_DIRECT\_GENERATION”, contains all necessary details required for the replication process. It is to be mentioned here that the cases discussed below, are outputs of the master node methodology, in which the positioning of the master node is at the centre, as dictated by the chord and thickness of respective cross sections (i.e. the positioning of master nodes at both cutout locations is not the same rather is as per the chord and thickness of blade at the respective locations).

#### *4.3.1 (A) Replicate complete stress state*

You require a minimum of 6-independent degrees of freedom at each load introduction end. In this way you are equipped with all deformations necessary to replicate a stress state completely. A sample is provided below:

***Table 9: Stress state comparison between complete blade and specimen (1).***

<pre> *** ** CUTOUT_LOC_1: 0.13000E+05 CUTOUT_LOC_2: 0.16000E+05 SENSOR'S X-COORDINATE: 0.14000E+05 UNIT OF STRESS:(MPa)  PRINT ELEMENT TABLE ITEMS PER ELEMENT  **** POST1 ELEMENT TABLE LISTING **** </pre> <table> <tr> <th>STAT</th><th>CURRENT</th><th>CURRENT</th><th>CURRENT</th><th>CURRENT</th><th>CURRENT</th><th>CURRENT</th></tr> <tr> <th>ELEM</th><th>SX_1</th><th>SY_1</th><th>SZ_1</th><th>SXY_1</th><th>SYZ_1</th><th>SXZ_1</th></tr> <tr> <td>11112</td><td>-8.7656</td><td>0.11160</td><td>-0.59536E-01</td><td>0.91854</td><td>0.13256</td><td>0.56343</td></tr> </table>							STAT	CURRENT	CURRENT	CURRENT	CURRENT	CURRENT	CURRENT	ELEM	SX_1	SY_1	SZ_1	SXY_1	SYZ_1	SXZ_1	11112	-8.7656	0.11160	-0.59536E-01	0.91854	0.13256	0.56343
STAT	CURRENT	CURRENT	CURRENT	CURRENT	CURRENT	CURRENT																					
ELEM	SX_1	SY_1	SZ_1	SXY_1	SYZ_1	SXZ_1																					
11112	-8.7656	0.11160	-0.59536E-01	0.91854	0.13256	0.56343																					
<i>Stress state from complete blade.</i>																											
<pre> *** ** CUTOUT_LOC_1: 0.13000E+05 CUTOUT_LOC_2: 0.16000E+05 SENSOR'S X-COORDINATE: 0.14000E+05 UNIT OF STRESS:(MPa)  PRINT ELEMENT TABLE ITEMS PER ELEMENT  **** POST1 ELEMENT TABLE LISTING **** </pre> <table> <tr> <th>STAT</th><th>MIXED</th><th>MIXED</th><th>MIXED</th><th>MIXED</th><th>MIXED</th><th>MIXED</th></tr> <tr> <th>ELEM</th><th>SX_1</th><th>SY_1</th><th>SZ_1</th><th>SXY_1</th><th>SYZ_1</th><th>SXZ_1</th></tr> <tr> <td>11112</td><td>-8.7656</td><td>0.11160</td><td>-0.59536E-01</td><td>0.91854</td><td>0.13256</td><td>0.56343</td></tr> </table>							STAT	MIXED	MIXED	MIXED	MIXED	MIXED	MIXED	ELEM	SX_1	SY_1	SZ_1	SXY_1	SYZ_1	SXZ_1	11112	-8.7656	0.11160	-0.59536E-01	0.91854	0.13256	0.56343
STAT	MIXED	MIXED	MIXED	MIXED	MIXED	MIXED																					
ELEM	SX_1	SY_1	SZ_1	SXY_1	SYZ_1	SXZ_1																					
11112	-8.7656	0.11160	-0.59536E-01	0.91854	0.13256	0.56343																					
<i>Stress state from specimen.</i>																											

As apparent this approach allows replication of a complete stress state but the problem is that generation of these deformations are not possible on the testing rig provided to us.

#### *4.3.1(B) possible load case- dual sided load introduction*

As described in the previous section, the lack of 5-degree of freedoms at the load introduction end prevents replication of complete stress state. Modelling the actual capability of the machine, meant application of two rotations (different

magnitudes) from either load introduction end, onto the subsections. From a practical stand point, the machine can bend the specimen with two different rotation angles, from either ends. The outcome is discussed below:

**Table 10: Stress state comparison between complete blade and specimen(2).**

<pre> CUTOUT_LOC_1: 0.13000E+05 CUTOUT_LOC_2: 0.16000E+05 SENSOR'S X-COORDINATE: 0.14000E+05 UNIT OF STRESS:(MPa)  PRINT ELEMENT TABLE ITEMS PER ELEMENT  ***** POST1 ELEMENT TABLE LISTING *****           CURRENT   CURRENT   CURRENT   CURRENT   CURRENT   CURRENT STAT      SX_1      SY_1      SZ_1      SXY_1      SYZ_1      SXZ_1 ELEM 11112 -8.7656      0.11160   -0.59536E-01 0.91854    0.13256    0.56343 </pre>						
<i>Stress state from complete blade.</i>						
<pre> CUTOUT_LOC_1: 0.13000E+05 CUTOUT_LOC_2: 0.16000E+05 SENSOR'S X-COORDINATE: 0.14000E+05 UNIT OF STRESS:(MPa)  PRINT ELEMENT TABLE ITEMS PER ELEMENT  ***** POST1 ELEMENT TABLE LISTING *****           CURRENT   CURRENT   CURRENT   CURRENT   CURRENT   CURRENT STAT      SX_5      SY_5      SZ_5      SXY_5      SYZ_5      SXZ_5 ELEM 11112 1.0479      0.57916    0.27042   -2.8653   -0.28228    0.50987 </pre>						
<i>Stress state from specimen.</i>						

Judging by the loading applied, the stress state in the X-axis (i.e. “SX<sub>5</sub>” in above table, highlighted in a green circle) should have been most accurate and as seen from the table it has the lowest error (i.e. 112 %) next to the shear in XZ (i.e. SXZ<sub>5</sub> in above table and amounts to 9.5 %). Although it is a lot but amongst all it is the best one.

The outcome is as expected, as the set of inputs we have provided contribute primarily to the stress along X-axis. The only one component missing from the set was an axial displacement.

#### 4.3.1 (C) preferable load case- Single sided load introduction.

On the other hand another possibility of loading is that you apply a fixation (fixed boundary condition) on one side of the subsection and load the other side with a difference of rotations from both ends of the subsection. In short, apply only the net effect on one side.

**Table 11: Stress state comparison between complete blade and specimen(3).**

CUTOUT_LOC_1: 0.13000E+05 CUTOUT_LOC_2: 0.16000E+05 SENSOR'S X-COORDINATE: 0.14000E+05 UNIT OF STRESS: (MPa)  PRINT ELEMENT TABLE ITEMS PER ELEMENT  ***** POST1 ELEMENT TABLE LISTING *****						
STAT	CURRENT	CURRENT	CURRENT	CURRENT	CURRENT	CURRENT
ELEM	SX_1	SY_1	SZ_1	SXY_1	SYZ_1	SXZ_1
11112	-8.7656	0.11160	-0.59536E-01	0.91854	0.13256	0.56343
<i>Stress state from complete blade.</i>						
CUTOUT_LOC_1: 0.13000E+05 CUTOUT_LOC_2: 0.16000E+05 SENSOR'S X-COORDINATE: 0.14000E+05 UNIT OF STRESS: (MPa)  PRINT ELEMENT TABLE ITEMS PER ELEMENT  ***** POST1 ELEMENT TABLE LISTING *****						
STAT	CURRENT	CURRENT	CURRENT	CURRENT	CURRENT	CURRENT
ELEM	SX_6	SY_6	SZ_6	SXY_6	SYZ_6	SXZ_6
11112	-0.49634	0.63437E-01	-0.10615E-01	-0.21609	0.68118E-02	0.95185E-01
<i>Stress state from specimen.</i>						

Looking into the cases discussed in (B) and (C), one often thinks that the end outcome should be the same and one must see the exact same stress state in “X” but the outputs dictate something else. The reason behind this is simply a matter of misinterpretation of the problem of the blade to the problem of a square cross section prismatic beam.

The blade’s cross section varies as you move along the span. To find multiple nodes with similar “Y” and “Z” coordinate across the complete span of the blade is unlikely. Rotations introduced via the master node approach would be translated to displacements to the slave nodes, which are closest in plane (YZ-Plane) to the master node. As the distances of nodes in “Y” and “Z” varies so does the displacements (which are actually outcome of applied rotations on the master node) but this is controlled by the algorithm programmed by ANSYS and cannot be altered. You only have control over the rotations that you apply to the master node.

While in case of a prismatic beam with a uniform mesh and both master nodes at the centre of the cross section would produce the same results for cases (B) and (C), as their closest in plane nodes would be at the same orthogonal distances. Nevertheless, this is a separate load.

#### *4.3.1(D) Single sided load introduction with axial displacement.*

Looking into the capability of the machine, there is a possibility of slight adjustment of the blade within the periphery of the “Threaded pallet” i.e. in the “Y” and “Z” axis (axis definition similar to that of the blade). This provides us, a mean to adjust the epicentre (master node) of the load introduction.

A review of kinematics and trigonometry dictates that the axial displacements of the blade could also be taken care of by adjusting the master node. Refer to the figure below for further clarification:



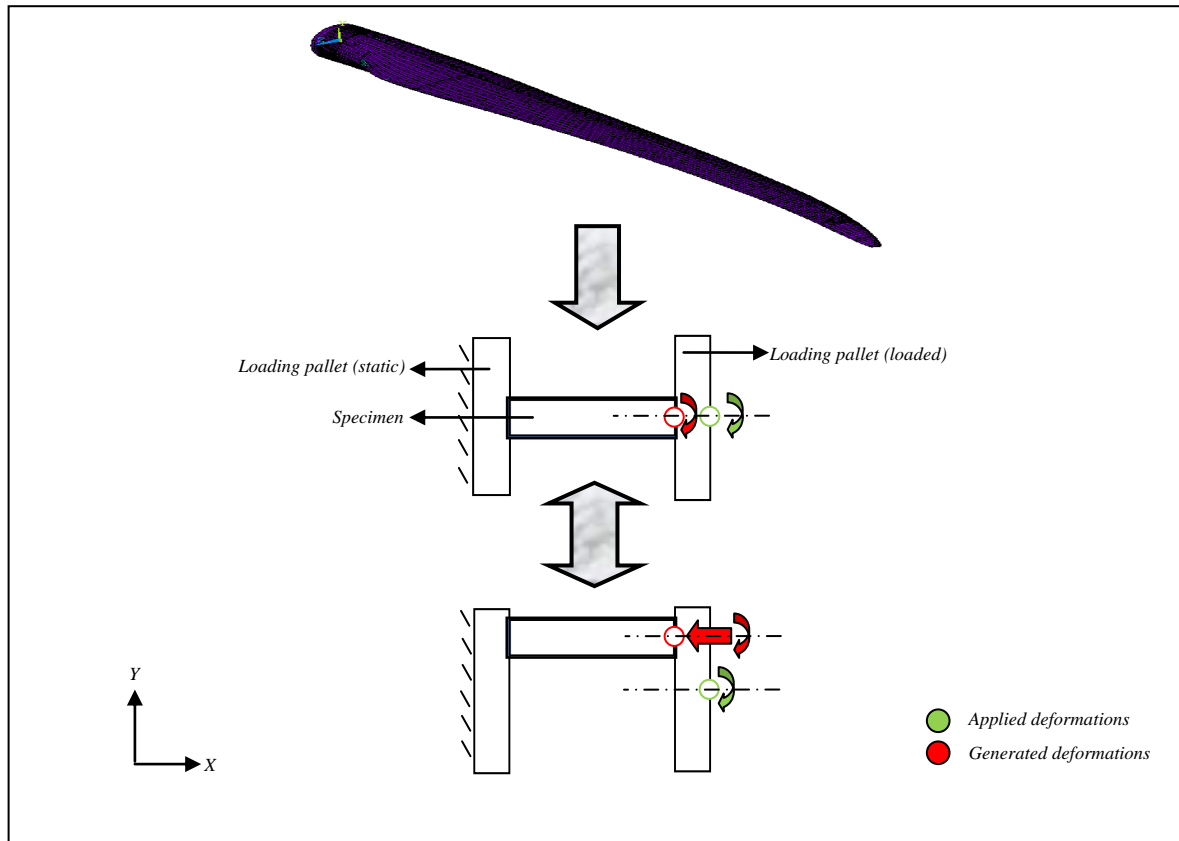


**Figure 27: Illustration of how axial deformation could be incorporated.**

From a practical point of view, this approach would be feasible if the adjustment lies within a reasonable range to which the pallets could be moved (within 100 centimetres in each direction). The methodology would be that the net rotations of the cross section (about “Y” and “Z” axis) would be recorded via the master nodes, and the master nodes would be readjusted to a point where there is zero axial displacement. In a sense, our stress state results from presence of two rotations and an axial displacement in our system would be replicated with presence of only two rotations within our system.

For this purpose a separate module of the program was extended and is called upon by not the main file but rather another sub class titled “GENERATE\_STRESS\_CONTOURS\_DIRECT\_GENERAT”. The outcome from the scripts were:

**Table 12: Stress state comparison between specimen, with and without axial deformation within the system.**

PRINT ELEMENT TABLE ITEMS PER ELEMENT						
***** POST1 ELEMENT TABLE LISTING *****						
STAT	CURRENT	CURRENT	CURRENT	CURRENT	CURRENT	CURRENT
ELEM	SX_2	SY_2	SZ_2	SXY_2	SYZ_2	SXZ_2
11018	20.903	0.19309	0.44599	-1.7826	0.11905	-1.1778

*Stress state of specimen with axial deformation included in the system.*

PRINT ELEMENT TABLE ITEMS PER ELEMENT						
***** POST1 ELEMENT TABLE LISTING *****						
STAT	MIXED	MIXED	MIXED	MIXED	MIXED	MIXED
ELEM	SX_2	SY_2	SZ_2	SXY_2	SYZ_2	SXZ_2
11018	35.956	0.33857	0.76402	-2.8894	0.19281	-2.0100

*Stress state of specimen without axial deformation included in the system.*

Observe the stress states along the “X-axis”(highlighted in a green circle) in above two figures. You observe an error of 75% between the two. To check the reason for such an error, a study was conducted and coupling was found to be the issue. Only a single rotation was applied about one of the axis (“Z” or “Y”) and the resulting rotation about the same axis was determined. There was a difference in applied rotations and recorded rotations. It was also observed that application of two rotations simultaneously resulted in such behaviour. See figure below:

**Table 13: Difference in applied and resulting rotations (two rotations applied simultaneously).**

<p>*** **</p> <p>MAX_Z NODAL COORDINATE 0.53420E+03</p> <p>MAX_Z NODAL DISPLACEMENT 0.99350E+01</p> <p>MIN_Z NODAL COORDINATE -0.36520E+03</p> <p>MAX_Z NODAL DISPLACEMENT 0.95797E+01</p> <p>M_Y: 0.39497E-03</p> <p>C_Y: 0.97240E+01</p> <p>NEW_Z_COORDINATE WITH ZERO TRANSLATION: -0.24619E+05</p> <p>APPLIED ROTATION ABOUT Y(rad): 0.27362E-03</p> <p>MEASURED TAN(THETA) ABOUT Y: 0.39497E-03</p> <p>CALCULATE ARCTAN AND CONVERT TO RADIAN TO COMPARE</p> <p>*** **</p>	<p>*** **</p> <p>MAX_Y NODAL COORDINATE -0.11380E+03</p> <p>MAX_Y NODAL DISPLACEMENT 0.77806E+01</p> <p>MIN_Y NODAL COORDINATE -0.33076E+03</p> <p>MAX_Y NODAL DISPLACEMENT 0.11255E+02</p> <p>M_Z: -0.16016E-01</p> <p>C_Z: 0.59580E+01</p> <p>NEW_Y_COORDINATE WITH ZERO TRANSLATION: 0.37200E+03</p> <p>APPLIED ROTATION ABOUT Z(rad): 0.15980E-01</p> <p>MEASURED TAN(THETA) ABOUT Z: 0.16016E-01</p> <p>CALCULATE ARCTAN AND CONVERT TO RADIAN TO COMPARE</p> <p>*** **</p>
---	--

The resulting angle about “Y” is “0.00039497” (radians). The resulting error is 44.3%. Similarly, the resulting angle recorded about the “Z” is “0.01601463” (radians). The resulting error is 0.22%.

Furthermore in our study, only a single rotation was applied about one of the axis (“Y” or “Z” axis) and the resulting rotation about the other axis was recorded (No axial displacement was applied) The results are presented in the plot below:

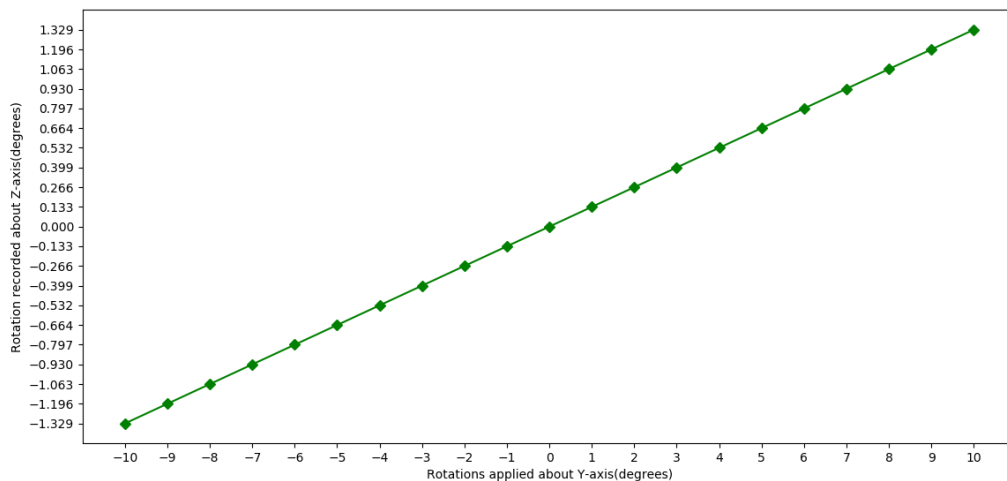


**Figure 28: Coupling identification(1).**

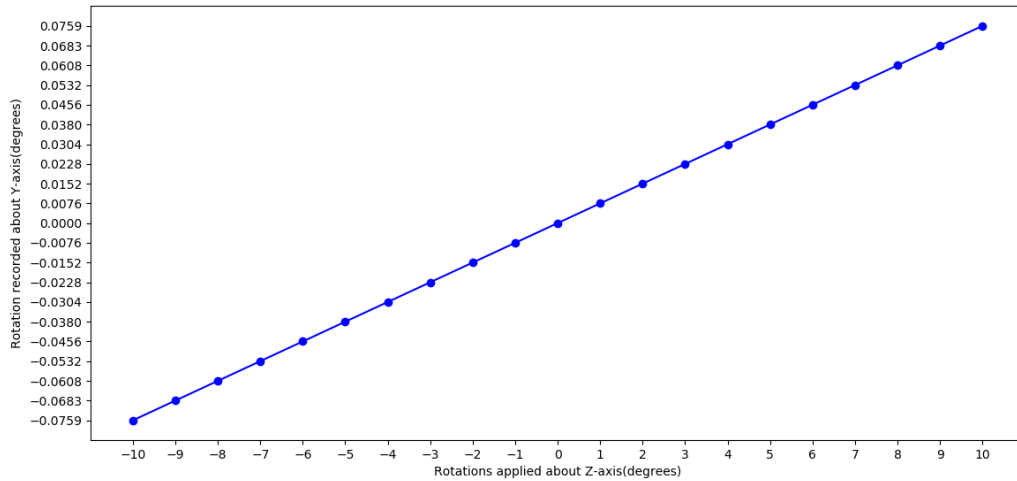


**Figure 29: Coupling identification(2).**

Evident from above figures, coupling exists within the model. This signifies that when combined rotations are applied to the specimen they would not act independently and would affect each other. It must be highlighted here that, if the rotation that was previously set to zero would take up a constant value and the other rotation would be varied again (from  $-10^{\circ}$  to  $+10^{\circ}$ ) the trend could differ. To avoid this problem, either a new methodology to deduce moments required to replicate the stress state (along X-axis) must be developed or this problem could be turned into a statistical problem (discussed further in the thesis).

The introduction of a sole axial displacement does not produce any rotations about “Y” or “Z”, which is as expected. The software indicates this by prompting an error of division by zero because the respective slopes of the deformed surfaces (cross sections) are zero and calculations for the alternate point with no axial displacements are halted. As shown in table below:

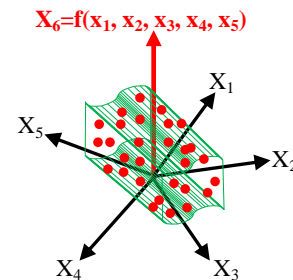
**Table 14: Measured rotations.**

<pre> *** ** MAX_Z NODAL COORDINATE 0.53420E+03 MAX_Z NODAL DISPLACEMENT 0.10000E+02 MIN_Z NODAL COORDINATE -0.36520E+03 MAX_Z NODAL DISPLACEMENT 0.10000E+02  M_Y: 0.00000E+00 C_Y: 0.10000E+02 NEW_Z_COORDINATE WITH ZERO TRANSLATION: 0.00000E+00  APPLIED ROTATION ABOUT Y(rad): 0.00000E+00 MEASURED TAN(THETA) ABOUT Y: 0.00000E+00 CALCULATE ARCTAN AND CONVERT TO RADIAN TO COMPARE *** ** </pre>	<pre> *** ** MAX_Y NODAL COORDINATE -0.11380E+03 MAX_Y NODAL DISPLACEMENT 0.10000E+02 MIN_Y NODAL COORDINATE -0.33076E+03 MAX_Y NODAL DISPLACEMENT 0.10000E+02  M_Z: 0.00000E+00 C_Z: 0.10000E+02 NEW_Y_COORDINATE WITH ZERO TRANSLATION: 0.00000E+00  APPLIED ROTATION ABOUT Z(rad): 0.00000E+00 MEASURED TAN(THETA) ABOUT Z: 0.00000E+00 CALCULATE ARCTAN AND CONVERT TO RADIAN TO COMPARE *** ** </pre>
Measured rotation about Y-axis under an axial load	Measured rotation about Z-axis under an axial load

#### 4.3.2 Function fitting and optimization

The fact that there is coupling in the model and can vary haphazardly to applied load cases lead us to the conclusion that only ANSYS APDL alone would not be enough to solve the problem. Although, ANSYS could be the first step to the solution. Further assistance would be required from a statistical tool capable of post-processing an output file from ANSYS. The required data set would be generated using ANSYS APDL and the post-processing would be done in tool (python / Java/ Matlab etc). A data set would be generated using ANSYS APDL. The data points would carry the following information:

- 1) Y-coordinate of master node. ( $x_1$ )
- 2) Z-coordinate of master node. ( $x_2$ )
- 3) Rotation about Y. ( $x_3$ )
- 4) Rotation about Z. ( $x_4$ )
- 5) Subcomponent length. ( $x_5$ )
- 6) Stress along the X-axis. ( $x_6$ )



There are two ways to approach the problem. One is in which you provide a polynomial and python fits the data to it and provides you with a residual value. Then depending upon the value you could decide to proceed on with the polynomial fit or to alter the provided polynomial to achieve a better fit. The other is that you provide “Python” with the data set and an “R-value” (Residual value) and python iterates and tries to fit a polynomial to the data set as per the R-value and provides you with the polynomial. The initial thought was to try both of them but due to lack of time only the first one was implemented and abandoned because to understand the coupling of basis with each other and to generate a polynomial manually was not possible so the code was scraped off and the second approach was tried but was left incomplete due to lack of time. Later on it was also conceived that to generate a reasonable data set the computation cost would be very high (for this study the “Y” and “Z” coordinate of master nodes at both cutout locations were kept the same). To accomplish such a task to achieve replication of stress state along the X-axis only, would have been an excellent numerical exercise but from a practical point of view did not seem as a viable option.

Alongside this, there was the problem of the basis. The discussion point was that whether to include the change in length into the basis as well. The decision lay upon what was the goal of the experiment being conducted. If the goal was to replicate the state of stress, as it was in the actual blade test then this would not be included into the basis. If the goal of the project was to replicate a state of stress at one specific point of the subsection then the change in length could be incorporated into the basis. Nevertheless, the length was included into the section and could be bypassed when required (the option has been programmed).

The master slave methodology is capable of providing inputs for the machine that would replicate the state of stress completely.

## Chapter-5: Conclusion & future work

A scaling scheme for testing of wind turbine blades was developed. The script was developed in ANSYS APDL and automated to maximum extent, allowing all possibilities of executing and by passing a certain section of code beforehand or during run time. The building block methodology was used to allow easy amendment and addition to the developed code. It is assumed that the model follows linear elastic behaviour, and no plasticity has been taken into account during development of transfer scheme. Post processing was done in Python. The research tasks considered and their results are summarized below:

Development of a transfer scheme, which would aid transfer of global loads from the wind turbine blade to local loads which would be applied to the subcomponent by the test bench. The transfer scheme is in form of a matrix.

The minimum degree of freedom of the test bench required for replication of a complete stress was determined to be six. Coupling was identified and could not be scaled into a fix factor as all bases behave differently to different load cases because of coupling.

The possibility of replication of a stress state along the X-axis on a test bench formerly present at the “German Aerospace centre” (DLR) was studied. Because of coupling the replication could not be achieved. All possibilities including dual and single sided loading (with and without axial deformation) were examined but failed to replicate the stress state.

An alternate solution to the coupling problem and to make possible the replication of the stress state along the X-axis was tried. A data set was generated in 5-Dimensional space (4-Dimensional if length of the specimen was not being considered) and a polynomial was fit through all points but the residual was perceived to be very high because the polynomial

was provided manually, without understanding how the basis interacted with one another in different load scenarios. This made it difficult to turn it into an optimization problem in which the design variable would have been the residual. This technique was abandoned.

Later on it was found that an alternate algorithm also exists in python that could provide you with the polynomial if it is given data points as input. This is where time became a constraint and the project was halted. For further progress in the project it is recommended to generate a polynomial from python. For a start, only one sided loading case could be studied and the understanding could be later on extended to the two sided loading case. The data set would be the value of stress along the X-Axis, which would be a function of four parameters i.e. the Y-coordinate of the master node, the Z-coordinate of the master node, the rotation applied about the Y-axis, the rotation applied about the Z-axis. The program would cycle through all possible variations and write description of coordinates, loads, and stresses in a single text file which would be read in python, the data would then be processed using “numpy” and “scipy” modules of “python”. A polynomial would be fit through the data. This polynomial would provide inputs for the test bench (positioning of loading pallets and the rotation/displacements to be applied) for replication of the stress state along the X-axis.



# Appendix

UNITS: (MPa)									
MATERIAL No.	E-X	E-Y	E-Z	PRXY	PRYZ	PRXZ	GXY	GYZ	GXZ
1.00	10.00	0.00	0.00	0.30	0.00	0.00	0.00	0.00	0.00
2.00	10.00	0.00	0.00	0.30	0.00	0.00	0.00	0.00	0.00
3.00	10.00	0.00	0.00	0.30	0.00	0.00	0.00	0.00	0.00
4.00	21888.00	9473.00	0.00	0.47	0.00	0.00	5126.00	5126.00	5126.00
5.00	10.00	0.00	0.00	0.30	0.00	0.00	0.00	0.00	0.00
6.00	10.00	0.00	0.00	0.30	0.00	0.00	0.00	0.00	0.00
7.00	44151.00	14526.00	0.00	0.30	0.00	0.00	3699.00	3699.00	3699.00
8.00	10.00	0.00	0.00	0.30	0.00	0.00	0.00	0.00	0.00
9.00	10.00	0.00	0.00	0.30	0.00	0.00	0.00	0.00	0.00
10.00	10.00	0.00	0.00	0.30	0.00	0.00	0.00	0.00	0.00
11.00	10.00	0.00	0.00	0.30	0.00	0.00	0.00	0.00	0.00
12.00	35.00	35.00	0.00	0.30	0.00	0.00	110.00	110.00	110.00
13.00	55.00	55.00	0.00	0.30	0.00	0.00	18.00	18.00	18.00
14.00	10.00	0.00	0.00	0.30	0.00	0.00	0.00	0.00	0.00
15.00	10.00	0.00	0.00	0.30	0.00	0.00	0.00	0.00	0.00
16.00	10.00	0.00	0.00	0.30	0.00	0.00	0.00	0.00	0.00
17.00	10.00	0.00	0.00	0.30	0.00	0.00	0.00	0.00	0.00
18.00	29873.00	13377.00	0.00	0.47	0.00	0.00	6918.00	6918.00	6918.00
19.00	55.00	55.00	0.00	0.30	0.00	0.00	18.00	18.00	18.00
20.00	10.00	0.00	0.00	0.30	0.00	0.00	0.00	0.00	0.00
21.00	10.00	0.00	0.00	0.30	0.00	0.00	0.00	0.00	0.00
22.00	11316.00	11316.00	0.00	0.63	0.00	0.00	11978.00	11978.00	11978.00
23.00	4864.00	0.00	0.00	0.33	0.00	0.00	0.00	0.00	0.00
24.00	26430.00	27520.00	0.00	0.12	0.00	0.00	3464.00	3464.00	3464.00
25.00	55.00	55.00	0.00	0.30	0.00	0.00	18.00	18.00	18.00
26.00	10.00	0.00	0.00	0.30	0.00	0.00	0.00	0.00	0.00
27.00	10.00	0.00	0.00	0.30	0.00	0.00	0.00	0.00	0.00
28.00	10.00	0.00	0.00	0.30	0.00	0.00	0.00	0.00	0.00
29.00	55.00	55.00	0.00	0.30	0.00	0.00	18.00	18.00	18.00
30.00	864.00	864.00	0.00	0.30	0.00	0.00	309.00	309.00	309.00
31.00	10.00	0.00	0.00	0.30	0.00	0.00	0.00	0.00	0.00
32.00	55.00	55.00	0.00	0.30	0.00	0.00	18.00	18.00	18.00
33.00	10.00	0.00	0.00	0.30	0.00	0.00	0.00	0.00	0.00
34.00	10.00	0.00	0.00	0.30	0.00	0.00	0.00	0.00	0.00
35.00	10.00	0.00	0.00	0.30	0.00	0.00	0.00	0.00	0.00
36.00	10.00	0.00	0.00	0.30	0.00	0.00	0.00	0.00	0.00
37.00	55.00	55.00	0.00	0.30	0.00	0.00	18.00	18.00	18.00

**Table 15: Material properties of 20-meter specimen.**

```

**RUN START**

TEST TYPE: FORCE CONTROLLED

ROOT CENTER IS GLOBAL ZERO
GENERATING MATRIX FOR X (mm):      2000.00
NUMBER OF NODES SELECTED ARE:-    106.00

MASTER NODE AT:
X (mm):  2000.00
Y (mm):   -3.52
Z (mm):   69.09

LOADING POINT DETAILS:
FORCE ATX (mm): 18000.00
FORCE ATY (mm): -551.80
FORCE ATZ (mm):  123.09

-DISTANCE BETWEEN MASTER AND LOAD IN X-DIRECTION: 16000.00
-DISTANCE BETWEEN MASTER AND LOAD IN Y-DIRECTION: -548.28
-DISTANCE BETWEEN MASTER AND LOAD IN Z-DIRECTION:   54.00

TRANSFER MATRICES:
MATRIX OF TRANSFORMATION (GLOBAL TO LOCAL)
-0.10000E+01 -0.21541E-09 -0.25337E-10  0.17660E-13  0.43202E-13 -0.41324E-13
 0.53232E-10 -0.10000E+01 -0.83240E-10  0.91543E-13 -0.15866E-12  0.85772E-13
 0.30739E-13  0.42620E-10 -0.10000E+01  0.19546E-12  0.19277E-12  0.54607E-15
-0.85290E-02  0.53875E+02  0.54828E+03 -0.99983E+00  0.21702E-03 -0.72935E-05
-0.54001E+02 -0.99782E-01  0.16000E+05  0.12816E-03 -0.99952E+00 -0.56234E-04
-0.54824E+03 -0.15999E+05  0.49336E-02 -0.81944E-03 -0.72191E-03 -0.10000E+01

INVERSE MATRIX IS (LOCAL TO GLOBAL)
-0.10000E+01 -0.44674E-09 -0.67644E-09 -0.17702E-13 -0.43257E-13  0.41327E-13
-0.14777E-10 -0.10000E+01  0.25735E-08 -0.91468E-13  0.15878E-12 -0.85781E-13
 0.10681E-10 -0.44593E-10 -0.10000E+01 -0.19552E-12 -0.19291E-12 -0.53380E-15
 0.16252E-01 -0.54001E+02 -0.55184E+03 -0.10002E+01 -0.21717E-03  0.73070E-05
 0.53996E+02 -0.80724E+00 -0.16008E+05 -0.12829E-03 -0.10005E+01  0.56262E-04
 0.54820E+03  0.16000E+05  0.12003E+02  0.81968E-03  0.72244E-03 -0.10000E+01

```

**Figure 30: Transfer matrix for force controlled test (X-coordinate: 2000)**

```

**RUN START**

TEST TYPE: FORCE CONTROLLED

ROOT CENTER IS GLOBAL ZERO
GENERATING MATRIX FOR X (mm):      4000.00
NUMBER OF NODES SELECTED ARE:-    104.00

MASTER NODE AT:
X (mm):  4000.00
Y (mm):  -14.92
Z (mm):  314.71

LOADING POINT DETAILS:
FORCE ATX (mm): 18000.00
FORCE ATY (mm): -551.80
FORCE ATZ (mm):  123.09

-DISTANCE BETWEEN MASTER AND LOAD IN X-DIRECTION: 14000.00
-DISTANCE BETWEEN MASTER AND LOAD IN Y-DIRECTION: -536.88
-DISTANCE BETWEEN MASTER AND LOAD IN Z-DIRECTION: -191.62

TRANSFER MATRICES:
MATRIX OF TRANSFORMATION (GLOBAL TO LOCAL)
-0.10000E+01 -0.39965E-09  0.14738E-10  0.39134E-14  0.50756E-13 -0.78283E-13
 0.10686E-09 -0.10000E+01 -0.29807E-09  0.46261E-13  0.24136E-12  0.22566E-12
-0.39030E-10 -0.58902E-09 -0.10000E+01  0.92615E-13  0.14904E-12 -0.11648E-12
-0.84022E-02 -0.19173E+03  0.53688E+03 -0.99983E+00  0.21697E-03 -0.70521E-05
 0.19161E+03 -0.97269E-01  0.14000E+05  0.12752E-03 -0.99952E+00 -0.56068E-04
-0.53784E+03 -0.13999E+05  0.28402E-02 -0.81789E-03 -0.72183E-03 -0.10000E+01

INVERSE MATRIX IS (LOCAL TO GLOBAL)
-0.10000E+01 -0.69554E-09 -0.72863E-09 -0.39846E-14 -0.50838E-13  0.78286E-13
-0.31740E-10 -0.10000E+01 -0.31052E-08 -0.46116E-13 -0.24132E-12 -0.22564E-12
-0.52213E-10 -0.10240E-08 -0.10000E+01 -0.92745E-13 -0.14921E-12  0.11649E-12
-0.36998E-01  0.19167E+03 -0.54001E+03 -0.10002E+01 -0.21711E-03  0.70656E-05
-0.19173E+03 -0.66354E+00 -0.14007E+05 -0.12765E-03 -0.10005E+01  0.56098E-04
 0.53798E+03  0.13999E+05  0.10549E+02  0.81812E-03  0.72236E-03 -0.10000E+01

```

**Figure 31: Transfer matrix for force controlled test (X-coordinate: 4000)**

```

**RUN START**

TEST TYPE: FORCE CONTROLLED

ROOT CENTER IS GLOBAL ZERO
GENERATING MATRIX FOR X (mm):      8000.00
NUMBER OF NODES SELECTED ARE:-    104.00

MASTER NODE AT:
X (mm):  8000.00
Y (mm):  -10.76
Z (mm):  323.40

LOADING POINT DETAILS:
FORCE ATX (mm): 18000.00
FORCE ATY (mm): -551.80
FORCE ATZ (mm):  123.09

-DISTANCE BETWEEN MASTER AND LOAD IN X-DIRECTION: 10000.00
-DISTANCE BETWEEN MASTER AND LOAD IN Y-DIRECTION: -541.04
-DISTANCE BETWEEN MASTER AND LOAD IN Z-DIRECTION: -200.31

TRANSFER MATRICES:
MATRIX OF TRANSFORMATION (GLOBAL TO LOCAL)
-0.10000E+01 -0.38729E-09  0.60622E-12  0.19292E-13  0.81604E-13 -0.84189E-13
 0.28632E-10 -0.10000E+01 -0.11988E-09 -0.14530E-12  0.32753E-13 -0.21698E-13
-0.24587E-10 -0.30184E-09 -0.10000E+01  0.11513E-12  0.10453E-12 -0.76833E-13
-0.77327E-02 -0.20041E+03  0.54103E+03 -0.99983E+00  0.21696E-03 -0.58858E-05
 0.20030E+03 -0.88043E-01  0.10000E+05  0.12456E-03 -0.99952E+00 -0.55273E-04
-0.54100E+03 -0.99995E+04  0.31433E-02 -0.80998E-03 -0.72229E-03 -0.10000E+01

INVERSE MATRIX IS (LOCAL TO GLOBAL)
-0.10000E+01 -0.45071E-09 -0.82817E-09 -0.19373E-13 -0.81709E-13  0.84193E-13
-0.46933E-10 -0.10000E+01 -0.12904E-09  0.14530E-12 -0.32753E-13  0.21699E-13
-0.37945E-10 -0.44341E-09 -0.10000E+01 -0.11522E-12 -0.10466E-12  0.76840E-13
-0.38944E-01  0.20038E+03 -0.54330E+03 -0.10002E+01 -0.21711E-03  0.58989E-05
-0.20043E+03 -0.43991E+00 -0.10005E+05 -0.12468E-03 -0.10005E+01  0.55301E-04
 0.54114E+03  0.99993E+04  0.76633E+01  0.81020E-03  0.72281E-03 -0.10000E+01

```

**Figure 32: Transfer matrix for force controlled test (X: 8000)**

```

**RUN START**

TEST TYPE: FORCE CONTROLLED

ROOT CENTER IS GLOBAL ZERO
GENERATING MATRIX FOR X (mm): 16000.00
NUMBER OF NODES SELECTED ARE:- 100.00

MASTER NODE AT:
X (mm): 16000.00
Y (mm): -377.80
Z (mm): 215.32

LOADING POINT DETAILS:
FORCE ATX (mm): 18000.00
FORCE ATY (mm): -551.80
FORCE ATZ (mm): 123.09

-DISTANCE BETWEEN MASTER AND LOAD IN X-DIRECTION: 2000.00
-DISTANCE BETWEEN MASTER AND LOAD IN Y-DIRECTION: -173.99
-DISTANCE BETWEEN MASTER AND LOAD IN Z-DIRECTION: -92.23

TRANSFER MATRICES:
MATRIX OF TRANSFORMATION (GLOBAL TO LOCAL)
-0.10000E+01 -0.96807E-11 -0.30143E-13 0.13847E-13 0.82772E-13 -0.15768E-13
0.21588E-12 -0.10000E+01 -0.36616E-11 -0.24506E-13 0.22335E-13 -0.10629E-13
-0.21261E-11 -0.36364E-10 -0.10000E+01 0.20842E-13 0.10499E-12 -0.35977E-13
-0.11306E-02 -0.92254E+02 0.17400E+03 -0.99986E+00 0.21843E-03 0.12883E-04
0.92231E+02 -0.26157E-01 0.20000E+04 0.63688E-04 -0.99952E+00 -0.39523E-04
-0.17499E+03 -0.19999E+04 -0.26272E-02 -0.71203E-03 -0.72780E-03 -0.10001E+01

INVERSE MATRIX IS (LOCAL TO GLOBAL)
-0.10000E+01 -0.20578E-10 -0.16804E-09 -0.13865E-13 -0.82827E-13 0.15770E-13
-0.41371E-11 -0.10000E+01 -0.36772E-10 0.24500E-13 -0.22348E-13 0.10630E-13
-0.13860E-10 -0.33658E-10 -0.10000E+01 -0.20877E-13 -0.10507E-12 0.35977E-13
-0.16774E-01 0.92292E+02 -0.17446E+03 -0.10001E+01 -0.21856E-03 -0.12875E-04
-0.92283E+02 -0.47020E-01 -0.20010E+04 -0.63756E-04 -0.10005E+01 0.39538E-04
0.17504E+03 0.19996E+04 0.15830E+01 0.71211E-03 0.72824E-03 -0.99990E+00

```

**Figure 33: Transfer matrix for force controlled test (X: 16000)**

```

**RUN START**

TEST TYPE: DISPLACEMENT CONTROLLED

ROOT CENTER IS GLOBAL ZERO
GENERATING MATRIX FOR X (mm):      2000.00
NUMBER OF NODES SELECTED ARE:-      88.00

MASTER NODE AT:
X (mm):  2000.00
Y (mm):   -3.52
Z (mm):   69.09

LOADING POINT DETAILS:
FORCE AT X (mm): 18000.00
FORCE AT Y (mm): -551.80
FORCE AT Z (mm):  123.09

-DISTANCE BETWEEN MASTER AND LOAD IN X-DIRECTION: 16000.00
-DISTANCE BETWEEN MASTER AND LOAD IN Y-DIRECTION: -548.28
-DISTANCE BETWEEN MASTER AND LOAD IN Z-DIRECTION:  54.00

TRANSFER MATRICES:
MATRIX OF TRANSFORMATION (GLOBAL TO LOCAL)
  0.22195E-01 -0.16346E-02 -0.65621E-03  0.66696E-04  0.11741E-03  0.21366E-02
-0.63115E-01  0.77070E-02  0.11320E-02 -0.91678E-04 -0.35151E-03 -0.61618E-02
-0.16041E-01  0.20493E-02  0.11246E-01 -0.55936E-03  0.13476E-04 -0.14702E-02
  0.48910E-05 -0.58121E-06 -0.10307E-05  0.85420E-06 -0.12104E-06  0.54927E-06
  0.14886E-04 -0.19262E-05 -0.11110E-04  0.55029E-06 -0.18298E-07  0.13618E-05
-0.52240E-04  0.69774E-05  0.65960E-06  0.60630E-07 -0.31201E-06 -0.50567E-05

INVERSE MATRIX IS (LOCAL TO GLOBAL)
  0.76796E+03  0.15607E+04 -0.74711E+04  0.17963E+06 -0.75497E+07 -0.14189E+07
-0.11672E+04 -0.21196E+04 -0.34553E+05 -0.45607E+06 -0.34921E+08  0.26812E+07
  0.81719E+02  0.19787E+03 -0.11192E+04  0.87224E+05 -0.12276E+07 -0.20235E+06
  0.19590E+06  0.20528E+06  0.37702E+07  0.40086E+08  0.38081E+10 -0.23358E+09
  0.10827E+07  0.11290E+07  0.20952E+08  0.21430E+09  0.21164E+11 -0.12870E+10
-0.73992E+05 -0.86224E+05 -0.12183E+07 -0.15216E+08 -0.12306E+10  0.94745E+08

```

**Figure 34: Transfer matrix for displacement controlled test (X: 2000)**

```

**RUN START**

TEST TYPE: DISPLACEMENT CONTROLLED

ROOT CENTER IS GLOBAL ZERO
GENERATING MATRIX FOR X (mm):    4000.00
NUMBER OF NODES SELECTED ARE:-    104.00

MASTER NODE AT:
X (mm):  4000.00
Y (mm):   -14.92
Z (mm):   314.71

LOADING POINT DETAILS:
FORCE AT X (mm): 18000.00
FORCE AT Y (mm):  -551.80
FORCE AT Z (mm):  123.09

-DISTANCE BETWEEN MASTER AND LOAD IN X-DIRECTION: 14000.00
-DISTANCE BETWEEN MASTER AND LOAD IN Y-DIRECTION:  -536.88
-DISTANCE BETWEEN MASTER AND LOAD IN Z-DIRECTION:  -191.62

TRANSFER MATRICES:
MATRIX OF TRANSFORMATION (GLOBAL TO LOCAL)
  0.50547E-01 -0.38447E-02 -0.54769E-02  0.36519E-03  0.22720E-03  0.48417E-02
-0.23974E+00  0.30482E-01  0.50602E-02 -0.80237E-03 -0.12496E-02 -0.23373E-01
-0.60273E-01  0.80817E-02  0.48312E-01 -0.24248E-02  0.11164E-03 -0.54890E-02
  0.82809E-05 -0.76983E-06 -0.36333E-05  0.26164E-05 -0.40942E-06  0.10298E-05
  0.14890E-04 -0.23535E-05 -0.20771E-04  0.10653E-05 -0.11536E-06  0.13066E-05
-0.11919E-03  0.16587E-04  0.77727E-06  0.26383E-06 -0.73091E-06 -0.11494E-04

INVERSE MATRIX IS (LOCAL TO GLOBAL)
-0.42690E+03  0.29389E+03 -0.24230E+04  0.16194E+06 -0.54885E+07 -0.22971E+06
-0.41641E+04 -0.12530E+04 -0.11515E+05 -0.30099E+06 -0.25813E+08  0.33316E+07
-0.85351E+02  0.31196E+02 -0.35278E+03  0.41647E+05 -0.84674E+06 -0.23436E+05
  0.48496E+06  0.13305E+06  0.12562E+07  0.28980E+08  0.28083E+10 -0.34433E+09
  0.26925E+07  0.73604E+06  0.69807E+07  0.15741E+09  0.15607E+11 -0.19080E+10
-0.16167E+06 -0.48603E+05 -0.40657E+06 -0.11455E+08 -0.90835E+09  0.12052E+09

```

**Figure 35: Transfer matrix for displacement controlled test  
(Xcoordinate4000)**

```

**RUN START**

TEST TYPE: DISPLACEMENT CONTROLLED

ROOT CENTER IS GLOBAL ZERO
GENERATING MATRIX FOR X (mm):      8000.00
NUMBER OF NODES SELECTED ARE:-      88.00

MASTER NODE AT:
X (mm):  8000.00
Y (mm):  -10.76
Z (mm):  323.40

LOADING POINT DETAILS:
FORCE AT X (mm): 18000.00
FORCE AT Y (mm): -551.80
FORCE AT Z (mm): 123.09

-DISTANCE BETWEEN MASTER AND LOAD IN X-DIRECTION: 10000.00
-DISTANCE BETWEEN MASTER AND LOAD IN Y-DIRECTION: -541.04
-DISTANCE BETWEEN MASTER AND LOAD IN Z-DIRECTION: -200.31

TRANSFER MATRICES:
MATRIX OF TRANSFORMATION (GLOBAL TO LOCAL)
  0.10428E+00 -0.72272E-02 -0.91852E-02  0.63387E-03  0.49327E-03  0.10018E-01
-0.11258E+01  0.15465E+00  0.12236E-01 -0.36476E-02 -0.58413E-02 -0.10924E+00
-0.92014E-01  0.16245E-01  0.17719E+00 -0.86364E-02  0.11081E-02 -0.77221E-02
  0.31194E-04 -0.31941E-05 -0.20129E-04  0.18539E-04 -0.30583E-05  0.46926E-05
-0.11326E-04  0.17427E-06 -0.40661E-04  0.20003E-05 -0.44083E-06 -0.12955E-05
-0.27803E-03  0.45915E-04 -0.14022E-05  0.13437E-05 -0.17978E-05 -0.26359E-04

INVERSE MATRIX IS (LOCAL TO GLOBAL)
-0.59248E+02  0.35312E+02 -0.29604E+03  0.94067E+04 -0.12700E+07 -0.18045E+05
-0.12341E+04 -0.15458E+03 -0.14257E+04 -0.70731E+05 -0.59752E+07  0.87035E+06
-0.19008E+02  0.28192E+01 -0.37084E+02  0.35448E+04 -0.18286E+06  0.15738E+04
  0.14804E+06  0.17801E+05  0.15557E+06  0.77007E+07  0.64925E+09 -0.93627E+08
  0.82151E+06  0.98512E+05  0.86446E+06  0.42332E+08  0.36080E+10 -0.51910E+09
-0.50008E+05 -0.64534E+04 -0.50388E+05 -0.27173E+07 -0.20999E+09  0.32301E+08

```

**Figure 36: Transfer matrix for displacement controlled test  
(Xcoordinate8000)**



```

**RUN START**

TEST TYPE: DISPLACEMENT CONTROLLED

ROOT CENTER IS GLOBAL ZERO
GENERATING MATRIX FOR X (mm): 16000.00
NUMBER OF NODES SELECTED ARE:- 100.00

MASTER NODE AT:
X (mm): 16000.00
Y (mm): -377.80
Z (mm): 215.32

LOADING POINT DETAILS:
FORCE AT X (mm): 18000.00
FORCE AT Y (mm): -551.80
FORCE AT Z (mm): 123.09

-DISTANCE BETWEEN MASTER AND LOAD IN X-DIRECTION: 2000.00
-DISTANCE BETWEEN MASTER AND LOAD IN Y-DIRECTION: -173.99
-DISTANCE BETWEEN MASTER AND LOAD IN Z-DIRECTION: -92.23

TRANSFER MATRICES:
MATRIX OF TRANSFORMATION (GLOBAL TO LOCAL)
0.22457E+00 0.19122E-01 -0.10098E-01 0.85562E-03 0.13814E-02 0.24480E-01
-0.29684E+01 0.85531E+00 -0.52031E-03 -0.38735E-04 -0.14240E-01 -0.25118E+00
0.47938E-01 0.24773E-02 0.77320E+00 -0.58470E-01 0.10811E-01 0.42003E-02
0.64615E-04 -0.18028E-04 -0.70070E-04 0.22169E-03 -0.38300E-04 0.27716E-04
-0.11234E-04 0.37398E-05 -0.10099E-03 -0.87913E-05 0.14811E-05 -0.17939E-05
0.22816E-03 0.11750E-03 0.29650E-06 0.10769E-04 0.77474E-06 0.41899E-04

INVERSE MATRIX IS (LOCAL TO GLOBAL)
0.14805E+02 0.49651E+00 -0.13434E+02 -0.73553E+04 -0.99239E+05 -0.37106E+04
-0.29618E+02 -0.31607E+00 -0.63645E+02 -0.36145E+05 -0.45915E+06 0.26042E+05
0.30172E+00 0.40472E-01 0.28659E+00 -0.21950E+03 -0.75860E+04 -0.14199E+03
0.61234E+04 0.19901E+03 0.69321E+04 0.39536E+07 0.49705E+08 -0.35668E+07
0.33891E+05 0.10998E+04 0.38509E+05 0.21937E+08 0.27615E+09 -0.19757E+08
-0.21981E+04 -0.73304E+02 -0.22422E+04 -0.12804E+07 -0.16054E+08 0.12532E+07

```

**Figure 37: Transfer matrix for displacement controlled test  
(Xcoordinate16000)**

```

**ROBUSTNESS TESTRUN START**
TYPE: DISPLACEMENT CONTROLLED
(ALL ROOT NODES ARE FIXED)
(MASS ELEMENT AT CUTOUT_LOC_2 WI BE THE LOADING POINT)

LOCATION OF MASS ELEMENT:
NODE NUMBER      33524.00
X_COORDINATE     16000.00
Y_COORDINATE     -377.80
Z_COORDINATE     215.32

NODE UNDER OBSERVATION: 24033.00

STRUCTURAL DISPLACEMENTS ARE:
      UX      UY      UZ
0.15055E+00 -0.26285E+01 0.38058E-02

**ROBUSTNESS TESTRUN END**

**ROBUSTNESS TESTRUN START**
TYPE: DISPLACEMENT CONTROLLED
(ALL ROOT NODES ARE FIXED)
(MASS ELEMENT AT CUTOUT_LOC_2 WI BE THE LOADING POINT)

LOCATION OF MASS ELEMENT:
NODE NUMBER      33526.00
X_COORDINATE     16000.00
Y_COORDINATE     -302.80
Z_COORDINATE     290.32

NODE UNDER OBSERVATION: 24033.00

STRUCTURAL DISPLACEMENTS ARE:
      UX      UY      UZ
0.15055E+00 -0.26285E+01 0.38058E-02

**ROBUSTNESS TESTRUN END**

```

**Figure 38:Robustness test output (type: displacement controlled, test load case from: first column of transfer matrix, amplification factor: 1)**

```

**ROBUSTNESS TESTRUN START**
TYPE: DISPLACEMENT CONTROLLED
(ALL ROOT NODES ARE FIXED)
(MASS ELEMENT AT CUTOUT_LOC_2 WI BE THE LOADING POINT)

LOCATION OF MASS ELEMENT:
NODE NUMBER      33524.00
X_COORDINATE     16000.00
Y_COORDINATE     -377.80
Z_COORDINATE     215.32

NODE UNDER OBSERVATION: 24033.00

STRUCTURAL DISPLACEMENTS ARE:
      UX      UY      UZ
-0.10943E-01  0.43858E+00  0.96766E-02

**ROBUSTNESS TESTRUN END**

**ROBUSTNESS TESTRUN START**
TYPE: DISPLACEMENT CONTROLLED
(ALL ROOT NODES ARE FIXED)
(MASS ELEMENT AT CUTOUT_LOC_2 WI BE THE LOADING POINT)

LOCATION OF MASS ELEMENT:
NODE NUMBER      33526.00
X_COORDINATE     16000.00
Y_COORDINATE     -302.80
Z_COORDINATE     290.32

NODE UNDER OBSERVATION: 24033.00

```

**Figure 39:Robustness test output (type: displacement controlled, test load case from: second column of transfer matrix, amplification factor: 1)**

```

**ROBUSTNESS TESTRUN START**
TYPE: DISPLACEMENT CONTROLLED
(ALL ROOT NODES ARE FIXED)
(MASS ELEMENT AT CUTOUT_LOC_2 WI BE THE LOADING POINT)

LOCATION OF MASS ELEMENT:
NODE NUMBER      33524.00
X_COORDINATE     16000.00
Y_COORDINATE     -377.80
Z_COORDINATE      215.32

NODE UNDER OBSERVATION: 24033.00

STRUCTURAL DISPLACEMENTS ARE:
      UX      UY      UZ
-0.44956E-01  0.34304E-01  0.39932E+00

**ROBUSTNESS TESTRUN END**

**ROBUSTNESS TESTRUN START**
TYPE: DISPLACEMENT CONTROLLED
(ALL ROOT NODES ARE FIXED)
(MASS ELEMENT AT CUTOUT_LOC_2 WI BE THE LOADING POINT)

LOCATION OF MASS ELEMENT:
NODE NUMBER      33526.00
X_COORDINATE     16000.00
Y_COORDINATE     -302.80
Z_COORDINATE      290.32

NODE UNDER OBSERVATION: 24033.00

```

**Figure 40:Robustness test output (type: displacement controlled, test load case from: third column of transfer matrix, amplification factor: 1)**

```

**ROBUSTNESS TESTRUN START**
TYPE: DISPLACEMENT CONTROLLED
(ALL ROOT NODES ARE FIXED)
(MASS ELEMENT AT CUTOUT_LOC_2 WI BE THE LOADING POINT)

LOCATION OF MASS ELEMENT:
NODE NUMBER      33524.00
X_COORDINATE     16000.00
Y_COORDINATE     -377.80
Z_COORDINATE     215.32

NODE UNDER OBSERVATION: 24033.00

STRUCTURAL DISPLACEMENTS ARE:
      UX      UY      UZ
0.85677E-03 -0.41213E-01 -0.15761E-01

**ROBUSTNESS TESTRUN END**

**ROBUSTNESS TESTRUN START**
TYPE: DISPLACEMENT CONTROLLED
(ALL ROOT NODES ARE FIXED)
(MASS ELEMENT AT CUTOUT_LOC_2 WI BE THE LOADING POINT)

LOCATION OF MASS ELEMENT:
NODE NUMBER      33526.00
X_COORDINATE     16000.00
Y_COORDINATE     -302.80
Z_COORDINATE     290.32

NODE UNDER OBSERVATION: 24033.00

```

**Figure 41:Robustness test output (type: displacement controlled, test load case from: fourth column of transfer matrix, amplification factor: 1)**

```

**ROBUSTNESS TESTRUN START**
TYPE: DISPLACEMENT CONTROLLED
(ALL ROOT NODES ARE FIXED)
(MASS ELEMENT AT CUTOUT_LOC_2 WI BE THE LOADING POINT)

LOCATION OF MASS ELEMENT:
NODE NUMBER      33524.00
X_COORDINATE     16000.00
Y_COORDINATE     -377.80
Z_COORDINATE     215.32

NODE UNDER OBSERVATION: 24033.00

STRUCTURAL DISPLACEMENTS ARE:
      UX      UY      UZ
0.70322E-03 -0.75520E-02 0.30335E-02

**ROBUSTNESS TESTRUN END**

**ROBUSTNESS TESTRUN START**
TYPE: DISPLACEMENT CONTROLLED
(ALL ROOT NODES ARE FIXED)
(MASS ELEMENT AT CUTOUT_LOC_2 WI BE THE LOADING POINT)

LOCATION OF MASS ELEMENT:
NODE NUMBER      33526.00
X_COORDINATE     16000.00
Y_COORDINATE     -302.80
Z_COORDINATE     290.32

NODE UNDER OBSERVATION: 24033.00

```

**Figure 42:Robustness test output (type: displacement controlled, test load case from: fifth column of transfer matrix, amplification factor: 1)**

```

**ROBUSTNESS TESTRUN START**
TYPE: DISPLACEMENT CONTROLLED
(ALL ROOT NODES ARE FIXED)
(MASS ELEMENT AT CUTOUT_LOC_2 WI BE THE LOADING POINT)

LOCATION OF MASS ELEMENT:
NODE NUMBER      33524.00
X_COORDINATE     16000.00
Y_COORDINATE     -377.80
Z_COORDINATE     215.32

NODE UNDER OBSERVATION: 24033.00

STRUCTURAL DISPLACEMENTS ARE:
      UX      UY      UZ
0.14155E-01 -0.25380E+00 0.27966E-02

**ROBUSTNESS TESTRUN END**

**ROBUSTNESS TESTRUN START**
TYPE: DISPLACEMENT CONTROLLED
(ALL ROOT NODES ARE FIXED)
(MASS ELEMENT AT CUTOUT_LOC_2 WI BE THE LOADING POINT)

LOCATION OF MASS ELEMENT:
NODE NUMBER      33526.00
X_COORDINATE     16000.00
Y_COORDINATE     -302.80
Z_COORDINATE     290.32

NODE UNDER OBSERVATION: 24033.00

```

**Figure 43:Robustness test output (type: displacement controlled, test load case from: sixth column of transfer matrix, amplification factor: 1)**

```

**ROBUSTNESS TEST START**
TYPE: FORCE CONTROLLED
(FIXED AT CUTOUT LOCATION-1)
(MASS ELEMENT AT CUTOUT_LOC_2 WI BE THE LOADING POINT)

LOCATION OF MASS ELEMENT:
NODE NUMBER      33524.00
X_COORDINATE     16000.00
Y_COORDINATE     -377.80
Z_COORDINATE     215.32

NODE UNDER OBSERVATION: 24033.00

NODAL DISPLACEMENTS (mm):
      UX      UY      UZ
-0.58219E-05 -0.11459E-03  0.98362E-05

**ROBUSTNESS TEST END**

**ROBUSTNESS TEST START**
TYPE: FORCE CONTROLLED
(FIXED AT CUTOUT LOCATION-1)
(MASS ELEMENT AT CUTOUT_LOC_2 WI BE THE LOADING POINT)

LOCATION OF MASS ELEMENT:
NODE NUMBER      33524.00
X_COORDINATE     16000.00
Y_COORDINATE     -277.80
Z_COORDINATE     315.32

NODE UNDER OBSERVATION: 24033.00

```

**Figure 44: Robustness test output (type: force controlled, test load case from: first column of transfer matrix, amplification factor: 1)**



```

**ROBUSTNESS TEST START**
TYPE: FORCE CONTROLLED
(FIXED AT CUTOUT LOCATION-1)
(MASS ELEMENT AT CUTOUT_LOC_2 WI BE THE LOADING POINT)

LOCATION OF MASS ELEMENT:
NODE NUMBER      33524.00
X_COORDINATE     16000.00
Y_COORDINATE     -377.80
Z_COORDINATE     215.32

NODE UNDER OBSERVATION: 24033.00

NODAL DISPLACEMENTS(mm):
      UX      UY      UZ
-0.38765E-04 -0.19679E-02  0.19445E-03

**ROBUSTNESS TEST END**

**ROBUSTNESS TEST START**
TYPE: FORCE CONTROLLED
(FIXED AT CUTOUT LOCATION-1)
(MASS ELEMENT AT CUTOUT_LOC_2 WI BE THE LOADING POINT)

LOCATION OF MASS ELEMENT:
NODE NUMBER      33524.00
X_COORDINATE     16000.00
Y_COORDINATE     -277.80
Z_COORDINATE     315.32

NODE UNDER OBSERVATION: 24033.00

```

**Figure 45: Robustness test output (type: force controlled, test load case from: second column of transfer matrix, amplification factor: 1)**

```

**ROBUSTNESS TEST START**
TYPE: FORCE CONTROLLED
(FIXED AT CUTOUT LOCATION-1)
(MASS ELEMENT AT CUTOUT_LOC_2 WI BE THE LOADING POINT)

LOCATION OF MASS ELEMENT:
NODE NUMBER      33524.00
X_COORDINATE     16000.00
Y_COORDINATE     -377.80
Z_COORDINATE     215.32

NODE UNDER OBSERVATION: 24033.00

NODAL DISPLACEMENTS(mm):
      UX      UY      UZ
0.20749E-03 -0.54626E-04 -0.70087E-03

**ROBUSTNESS TEST END**

**ROBUSTNESS TEST START**
TYPE: FORCE CONTROLLED
(FIXED AT CUTOUT LOCATION-1)
(MASS ELEMENT AT CUTOUT_LOC_2 WI BE THE LOADING POINT)

LOCATION OF MASS ELEMENT:
NODE NUMBER      33524.00
X_COORDINATE     16000.00
Y_COORDINATE     -277.80
Z_COORDINATE     315.32

NODE UNDER OBSERVATION: 24033.00

```

**Figure 46: Robustness test output (type: force controlled, test load case from: third column of transfer matrix, amplification factor: 1)**

```

**ROBUSTNESS TEST START**
TYPE: FORCE CONTROLLED
(FIXED AT CUTOUT LOCATION-1)
(MASS ELEMENT AT CUTOUT_LOC_2 WI BE THE LOADING POINT)

LOCATION OF MASS ELEMENT:
NODE NUMBER      33524.00
X_COORDINATE     16000.00
Y_COORDINATE     -377.80
Z_COORDINATE     215.32

NODE UNDER OBSERVATION: 24033.00

NODAL DISPLACEMENTS(mm):
      UX      UY      UZ
0.34642E-07  0.86040E-06 -0.82220E-07

**ROBUSTNESS TEST END**

**ROBUSTNESS TEST START**
TYPE: FORCE CONTROLLED
(FIXED AT CUTOUT LOCATION-1)
(MASS ELEMENT AT CUTOUT_LOC_2 WI BE THE LOADING POINT)

LOCATION OF MASS ELEMENT:
NODE NUMBER      33524.00
X_COORDINATE     16000.00
Y_COORDINATE     -277.80
Z_COORDINATE     315.32

NODE UNDER OBSERVATION: 24033.00

```

**Figure 47: Robustness test output (type: force controlled, test load case from: fourth column of transfer matrix, amplification factor: 1)**

```

**ROBUSTNESS TEST START**
TYPE: FORCE CONTROLLED
(FIXED AT CUTOUT LOCATION-1)
(MASS ELEMENT AT CUTOUT_LOC_2 WI BE THE LOADING POINT)

LOCATION OF MASS ELEMENT:
NODE NUMBER      33524.00
X_COORDINATE     16000.00
Y_COORDINATE     -377.80
Z_COORDINATE     215.32

NODE UNDER OBSERVATION: 24033.00

NODAL DISPLACEMENTS (mm):
      UX      UY      UZ
-0.29750E-07 -0.47892E-07  0.80782E-07

**ROBUSTNESS TEST END**

**ROBUSTNESS TEST START**
TYPE: FORCE CONTROLLED
(FIXED AT CUTOUT LOCATION-1)
(MASS ELEMENT AT CUTOUT_LOC_2 WI BE THE LOADING POINT)

LOCATION OF MASS ELEMENT:
NODE NUMBER      33524.00
X_COORDINATE     16000.00
Y_COORDINATE     -277.80
Z_COORDINATE     315.32

NODE UNDER OBSERVATION: 24033.00

```

**Figure 48: Robustness test output (type: force controlled, test load case from: fifth column of transfer matrix, amplification factor: 1)**

```

**ROBUSTNESS TEST START**
TYPE: FORCE CONTROLLED
(FIXED AT CUTOUT LOCATION-1)
(MASS ELEMENT AT CUTOUT_LOC_2 WI BE THE LOADING POINT)

LOCATION OF MASS ELEMENT:
NODE NUMBER      33524.00
X_COORDINATE     16000.00
Y_COORDINATE     -377.80
Z_COORDINATE     215.32

NODE UNDER OBSERVATION: 24033.00

NODAL DISPLACEMENTS(mm):
      UX      UY      UZ
-0.27814E-08 -0.19919E-06  0.19273E-07

**ROBUSTNESS TEST END**

**ROBUSTNESS TEST START**
TYPE: FORCE CONTROLLED
(FIXED AT CUTOUT LOCATION-1)
(MASS ELEMENT AT CUTOUT_LOC_2 WI BE THE LOADING POINT)

LOCATION OF MASS ELEMENT:
NODE NUMBER      33524.00
X_COORDINATE     16000.00
Y_COORDINATE     -277.80
Z_COORDINATE     315.32

NODE UNDER OBSERVATION: 24033.00

NODAL DISPLACEMENTS(mm):
      UX      UY      UZ
-0.27814E-08 -0.19919E-06  0.19273E-07

**ROBUSTNESS TEST END**

```

**Figure 49: Robustness test output (type: force controlled, test load case from: sixth column of transfer matrix, amplification factor: 1)**

## Bibliography

- [1] wind turbine. (n.d.), American Heritage® Dictionary of the English Language, Fifth Edition (2011).
- [2] Garate, J., Solovitz, S.A. & Kim, D. (2018). Fabrication and Performance of Segmented Thermoplastic Composite Wind Turbine Blades. *International Journal of Precision Engineering and Manufacturing-Green Technology*. 5, pp.271–277.
- [3] Jensen, F.M. (2013), *Advances in Wind Turbine Blade Design and Materials*, Woodhead publishing limited.
- [4] Fraunhofer IWES. (2018), SmartBlades2.
- [5] Jensen, F. M., Kling, A., & Sørensen, J. D. (2012). Scale-up of wind turbine blades - Changes in failure type. *European Wind Energy Conference and Exhibition 2012*.
- [6] Lamarre, A. (2017), Improved inspection of composite wind turbine blades with accessible advanced ultrasonic phased array technology, *15th Asia Pacific Conference for Non-Destructive Testing (APCNDT2017)*.
- [7] Sundaresan, M.J. Schulz, M.J. & Ghoshal, A. (1999) ,Structural Health Monitoring Static Test of a Wind Turbine Blade, *Intelligent Structures and Mechanisms (ISM) Laboratory, Department of Mechanical Engineering, North Carolina A&T State University*.
- [8] Froese, M. (2017, January 4). How are blade materials and manufacturing changing to keep up with larger turbines. Retrieved from <https://www.windpowerengineering.com/blade-materials-manufacturing-changing-keep-larger-turbines/>.
- [9] Mishnaevsky, L. Branner, K. Petersen, H. N. Beauson, J. McGugan, M. & Sørensen, B. F. (2017). *Materials for Wind Turbine Blades: An Overview*. Materials (Basel, Switzerland), 10(11), 1285. <https://doi.org/10.3390/ma10111285>.
- [10] Nussen, R.P.L. Van Delft, D.R.V. (2003), *Alternative Fatigue Formulations for Variable Amplitude Loading of Fibre Composites for Wind Turbine Rotor Blades*, *European Structural Integrity Society*, 32, 563-574.
- [11] Liu, H. Zhao, R. & Zheng, Y. (2014, 24 July), Optimization Method for Girder of Wind Turbine Blade, *Mathematical Problems in Engineering*, 2014,1-5,” doi: 10.1155/2014/898736.
- [12] Jørgensen . Bjørn, J. (2017), *Adhesive Joints in Wind Turbine Blades (Doctoral thesis)*, Available from Technical University of Denmark Library, DTU:00000027 (Or doi: 0.11581/).
- [13] Comsol Multiphysics, Forrister, T. (2018 November 14), *Analyzing Wind Turbine Blades with the Composite Materials Module*.
- [14] Sompong, N. (2017, June), Effects of bend-twist coupling deformation on the aerodynamic performance of a wind turbine blade, *International Journal of GEOMATE*, 34(34), pp 15-20.

- [15] Reddy, N.J. (1993), Introduction to the Finite Element Method, Texas A & M university.pdf.
- [16] Meschke, G. (2011, October), Finite Element Methods in Linear Structural Mechanics, Ruhr University Bochum.
- [17] SAS IP Inc (Release 14.0). (2011), Chapter-2: Element classifications, 2.2. Summary of Element Types, SOLID186.
- [18] Reddy, S.B. Kumar, S.J. Reddy, E.C. & Reddy, K.V.K. (2013), Influence of rotary inertia and shear on flexural motions of isotropic, elastic plates, Journal of Composites, 18, pp. 31–38, 1951.
- [19] SAS IP Inc (Release 14.0). (2011), Chapter -2: Element classifications, 2.2. Summary of Element Types, Shell 281.
- [20] SAS IP Inc (Release 14.0). (2011), Section 11.5. How to Create Constraint Equations. [Dated: 2019, March 20].
- [21] SAS IP Inc (Release 14.5). (2012), ANSYS Mechanical APDL Modeling and Meshing Guide.
- [22] Chang, S-C. Lin T-W. (1988), Constraint relation implementation for finite element analysis from an element basis, Advances in Engineering Software(1978), 10(4), pages 191-194.
- [23] SAS IP Inc (Release 14.0) (2011), Modeling a Shell-Solid Assembly [Dated: 2019, March 25].
- [24] SAS IP Inc (Release 13.0). (2010) , Chapter 2. Command groupings, Section 2.5. PREP7 Commands.
- [25] Hibbeler, C.R. (2018), Statics and Mechanics of Materials, Pearson Education Limited.